

Disparities in particulate matter (PM₁₀) origins and oxidative potential at a city-scale (Grenoble, France) - Part I: Source apportionment at three neighbouring sites

Lucille Joanna S. Borlaza¹, Samuël Weber¹, Gaëlle Uzu^{1*}, Véronique Jacob¹, Trishalee Cañete¹, Steve Micallef⁴, Cécile Trébuchon⁴, Rémy Slama⁵, Olivier Favez^{2,3}, and Jean-Luc Jaffrezo¹

¹University Grenoble Alpes, CNRS, IRD, INP-G, IGE (UMR 5001), 38000 Grenoble, France

²INERIS, Parc Technologique Alata, BP 2, 60550 Verneuil-en-Halatte, France

³Laboratoire Central de Surveillance de la Qualité de l'Air (LCSQA), 60550 Verneuil-en-Halatte, France

⁴Atmo Auvergne-Rhône Alpes, 38400 Grenoble, France

⁵IAB, Team of Environmental Epidemiology applied to Reproduction and Respiratory Health, University of Grenoble Alpes, 38000 Grenoble, France

*Correspondence to: Gaëlle Uzu (gaelle.uzu@ird.fr)

Abstract. A fine-scale source apportionment of PM₁₀ was conducted in three different urban sites (background, hyper-center, and peri-urban) within 15 km of the city in Grenoble, France using Positive Matrix Factorization (PMF 5.0) on measured chemical species from collected filters (24-hr) from February 2017 to March 2018. To improve the PMF solution, several new organic tracers (3-MBTCA, pinic acid, phthalic acid, MSA, and cellulose) were additionally used in order to identify sources that are commonly unresolved by classic PMF methodologies. An 11-factor solution was obtained in all sites including commonly identified sources from primary traffic (13%), nitrate-rich (17%), sulfate-rich (17%), industrial (1%), biomass burning (22%), aged sea salt (4%), sea/road salt (3%), and mineral dust (7%), and the newly found sources from primary biogenic (4%), secondary biogenic oxidation (10%), and MSA-rich (3%). Generally, the chemical species exhibiting similar temporal trends and strong correlations showed uniformly distributed emission sources in the Grenoble basin. The improved PMF model was able to obtain and differentiate chemical profiles of specific sources even at high proximity of receptor locations confirming its applicability in a fine-scale resolution. In order to test the similarities between the PMF-resolved sources, the Pearson distance and standardized identity distance (PD-SID) of the factors in each site were compared. The PD-SID metric determined whether a given source is homogeneous (i.e. with similar chemical profiles) or heterogeneous over the 3 sites, thereby allowing to better discriminate localized characteristics of specific sources. Overall, the addition of the new tracers allowed the identification of substantial sources (especially in the SOA fraction) that would not have been identified or possibly mixed with other factors, resulting in an enhanced resolution and sound source profile of urban air quality at a city scale.

31 **1 Introduction**

32 Atmospheric aerosols, or particulate matter (PM), are complex mixtures of particles from direct and indirect emissions (e.g.,
33 gas-to-particle conversion processes) that are from natural and anthropogenic sources in the atmosphere (Wilson and Spengler,
34 1996). The growing interest in ambient aerosol studies is driven by their impacts on health, air quality, and global climate
35 (Colette et al., 2008; Horne and Dabdub, 2017; McNeill, 2017; Shiraiwa et al., 2017). Numerous epidemiological studies have
36 established consistent associations between PM and various health diseases, especially cardiorespiratory illnesses (Brunekreef,
37 2005; Franchini and Mannucci, 2009; Langrish et al., 2012; Ostro et al., 2011; Willers et al., 2013). Once inhaled, PM notably
38 have the capacity to generate reactive oxygen species (ROS), which leads to pro-inflammatory responses that can ultimately
39 result in apoptosis (Ayres et al., 2008; Jin et al., 2018; Nel, 2005; Piao et al., 2018; Yang et al., 2018). Investigating the PM
40 oxidative potential (OP) in light of their major emission sources at various urban environments can then provide valuable
41 information to instigate air pollution abatement policies limiting health outcomes. However, spatially-resolved PM source
42 apportionment at a city-scale remains a challenging task (Dai et al., 2020b, 2020a; Pandolfi et al., 2020).

43 Receptor models demonstrated their ability to extract information by variable reduction techniques, especially in large datasets,
44 in different branches of scientific research. In particular, the Positive Matrix Factorization (PMF) model is widely used in
45 many studies to determine the contribution of emission sources in PM, based on the characterization of chemical tracers in a
46 series of PM samples (Belis et al., 2014, 2020; Hopke, 2016; Pindado and Perez, 2011; Saeaw and Thepanondh, 2015; Weber
47 et al., 2019). The option of refining source profiles by adding constraints have further improved the accuracy of identifying
48 sources (Charron et al., 2019; Marmur et al., 2007; Weber et al., 2019; Zhu et al., 2018), especially when specific chemical
49 species and unique tracers are included (Bullock et al., 2008; Wang et al., 2017a; Yan et al., 2017; Zhang et al., 2010). In fact,
50 the PMF model has shown good strengths in both rural and urban environments (Pindado and Perez, 2011; Schauer and Cass,
51 2000), however, there are limited studies in cities at a fine-scale resolution that allows the assessment of local variabilities in
52 a metropolitan area.

53 The city of Grenoble (France), with a complex topography and marked seasonal cycles of particulate pollution, offers
54 interesting opportunities to explore the capability of PMF to resolve both the small spatial and large temporal scales of
55 variabilities of the contribution of PM sources with the possibility of using additional tracers. Specific meteorological
56 conditions, topography, and local sources impact the local PM chemistry in the atmosphere thereby requiring additional sources
57 to properly scrutinize these local variations in urban environments. Further, previous works were already conducted in the area
58 using extended PMF (Srivastava et al., 2018b; Weber et al., 2019), providing useful benchmark indicators.

59 The application of PMF requires to accurately consider a wide range of chemical components in PM, particularly for its
60 organic fraction (Seinfeld and Pankow, 2003), consisting of complex mixtures especially in urban environments (Schauer and
61 Cass, 2000; Zheng et al., 2004). In fact, around 80% of organic matter (OM) generally remains unidentified at the molecular
62 level (Chevrier, 2016; Golly et al., 2019) resulting in misclassification or several un-apportioned sources of PM₁₀. Additionally,
63 the difference in formation pathways of PM components may limit the identification of sources of PM, especially the secondary

64 organic carbon (SOC) fraction, without the use of relevant organic tracers (Srivastava et al., 2018b; Wang et al., 2017a).
65 Different organic tracers have already been integrated in previous PMF studies, allowing to resolve specific sources of organic
66 aerosols that cannot be easily identified, such as primary biogenic aerosols and products of secondary processes in the
67 atmosphere (Waked et al., 2014; Belis et al., 2019; Golly et al., 2019; Hu et al., 2010; Weber et al., 2019).

68 In particular, Srivastava et al., 2018b was able to differentiate between different types of primary and secondary organic
69 fractions at a Grenoble urban background site, after analysing about 150 organic markers (and selecting 25 of them for the
70 final PMF run). Such studies are highly labour-intensive and often require the use of costly analytical devices and methods,
71 whereas some of the missing key molecular markers might still be obtained using simpler and/or more targeted techniques.
72 Moreover, the usefulness of these organic tracers in PMF analysis requires extensive methodological exploration, in terms of
73 their applicability as source tracers considering the much lower variability of their concentrations compared to other traditional
74 tracers.

75 In this paper, we present results of a study conducted over one year at three sites within 15 km of each other in the Grenoble
76 metropolitan area within the framework of the Mobil'Air project (available in <https://mobilair.univ-grenoble-alpes.fr/>, last
77 access: 02 November 2020). The sources of PM₁₀ were apportioned considering major chemical components contributing to
78 the PM mass, including organic and elemental carbon, ions, a condensed set of commonly-used organic markers (anhydride
79 monosaccharides, polyols, MSA), and metals. Additional fit-for-purpose tracers, including free cellulose and several organic
80 acids, were also added in the PMF input datasets to tackle specific sources that are difficult to discriminate using a traditional
81 PMF dataset only. Results obtained from this improved PMF analysis were then used to investigate the spatial and seasonal
82 variabilities in the source contributions for different urban typologies inside a metropolitan area. The overall outputs of this
83 study could be of interest to policy makers in providing vital information for designing effective particulate matter control
84 strategies including the setup of low emission zones and an opportunity to acquire more knowledge about the associations of
85 these emissions to other emerging health-based metrics (e.g., OP of PM) at a city scale as presented in the companion paper
86 (Borlaza et al., 2021).

87 **2 Methodology**

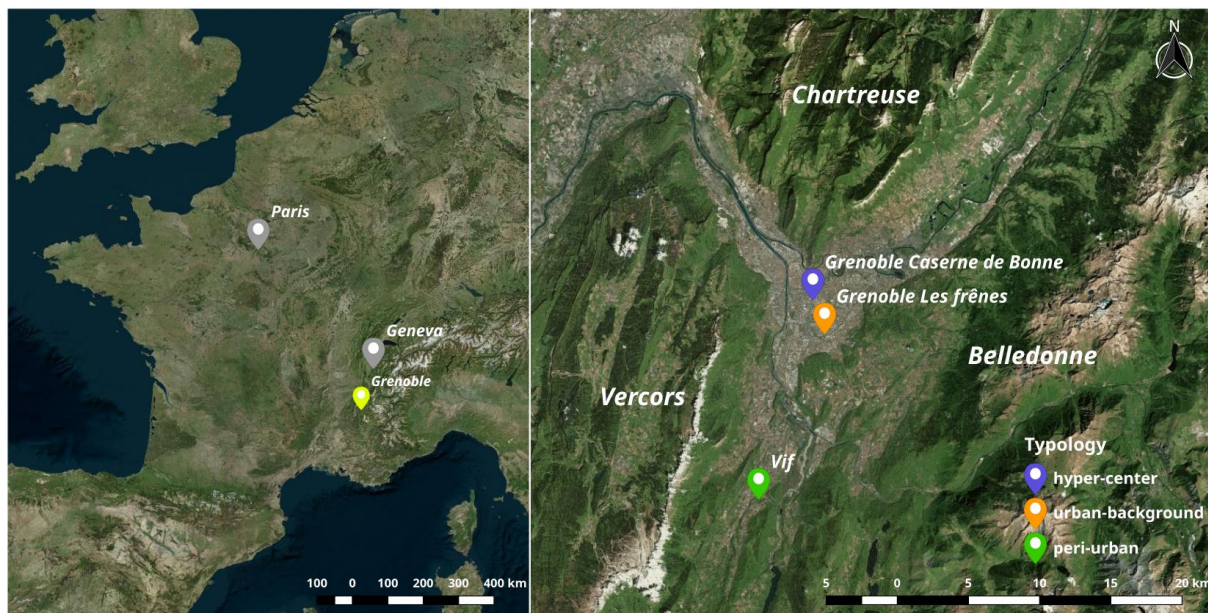
88 **2.1 PM₁₀ sample collection**

89 The metropolitan area of Grenoble, regarded as the capital of the French Alps, has a population of about 440,000 inhabitants.
90 The city itself presents a low altitude range (between 204 and 600 meters above sea level or masl) but is located in an alpine
91 environment (Figure 1), surrounded by several mountain ranges, including Chartreuse (north), Vercors (south and west), and
92 Belledonne (east). These mountains restrict the movement of air heavily affecting the local meteorology and favouring the
93 development of atmospheric temperature inversions with entrapment of pollutants in the valley, particularly in the winter
94 (Bessagnet et al., 2020). The topography within the Grenoble basin and seasonality of particulate air pollution in the city makes
95 it an ideal location to explore both the small- and large-scale variabilities of PM sources. During this study, a PM₁₀ sampling

96 campaign was conducted in the Grenoble area at three sites selected to represent various urban typologies, including: Les
97 Frênes (LF, urban background site, 214 masl), Caserne de Bonne (CB, urban hyper-center, 212 masl), and Vif (peri-urban
98 area, 310 masl). These sites are all within a 15-km range from the city center. LF is a long-standing reference urban background
99 site for the regional air quality monitoring network (Atmo Auvergne Rhône-Alpes), nearby a park at the outer fringe of the
100 city. Vif is a peri-urban site, with suburban housings close to rural areas. However, this site could potentially receive industrial
101 emissions from a nearby chemical industrial area (<6 km) in the air flux within this North – South valley. Substantial influence
102 of biogenic emissions could also be expected as this site is in-between the foot of Vercors and Belledune national parks. Lastly,
103 while in a pedestrian area, the site of CB is in the hyper-center of Grenoble and exposed to traffic emissions from the nearby
104 boulevards.

105 The daily (24-h) PM₁₀ sampling collection was conducted from February 28, 2017 to March 10, 2018 (starting at 00:00 local
106 time) with an average 3-day sampling interval. A total of 125, 127 and 127 samples were collected during this year-long
107 campaign at LF, CB, and Vif, respectively. The PM₁₀ collection was performed using high volume samplers (Digitel DA80,
108 30 m³ h⁻¹) onto 150 mm-diameter pure quartz fibre filters (Tissu-quartz PALL QAT-UP 2500 diameter 150 mm). All filter
109 handling procedures of filters were strictly under quality control assurance procedures to avoid any possible contamination. In
110 particular, filters were preheated at 500 °C for 12 hours before use to avoid organic contamination. At least 20 field blank
111 filters were collected at each site to determine detection limits (DL) and to check for the absence of contamination during
112 sample transport, setup, and recovery. After particle collection, filter samples were wrapped in aluminium foil, sealed in zipper
113 plastic bags, and stored at <4 °C until further chemical analysis. Complementary measurements at the sampling sites notably
114 included the total PM₁₀ mass concentration measured using tapered element oscillating microbalances equipped with filter
115 dynamics measurement systems (TEOM-FDMS) (Grover, 2005).

116



117
 118 **Figure 1: Grenoble, the city where the sampling was made, placed on a European Map (left), and PM monitoring sites (right): Les**
 119 **Frênes or LF (background), Caserne de Bonne or CB (hyper-center), and Vif (peri-urban). Image credit: Bing™ Aerial. © Microsoft**

120
 121 **2.2 Classical set of chemical analyses**

122 Sampled filters were subjected to various chemical analyses for the quantification of the major chemical constituents and
 123 specific chemical tracers of sources needed for PMF studies.

124 The carbonaceous fractions (organic carbon (OC) and elemental carbon (EC)) were analysed with a Sunset Lab analyser
 125 (Aymoz et al., 2007; Birch and Cary, 1996) using the EUSAAR2 thermo-optical protocol (Cavalli et al., 2010). Total organic
 126 matter (OM) in daily ambient aerosols were estimated by multiplying the OC mass by a fixed conversion factor of 1.8 based
 127 on findings obtained from previous studies (Favez et al., 2010; Putaud et al., 2010).

128 A solid/liquid extraction was performed on 11.34 cm² punches soaked in a 10 ml of ultra-pure water under vortex agitation for
 129 20 minutes. The extract was then filtered with a 0.25 µm porosity Acrodisc (Milipore Millex-EIMF) filter. The major ionic
 130 components were measured by ion chromatography (IC) following a standard protocol described in Jaffrezou et al. (1998) and
 131 Waked et al. (2014), using an ICS3000 dual channel chromatograph (Thermo-Fisher) with AS11HC column for the anions
 132 and CS12 for the cations. This technique allowed the quantification of sodium (Na⁺), ammonium (NH₄⁺), potassium (K⁺),
 133 magnesium (Mg²⁺), calcium (Ca²⁺), chloride (Cl⁻), nitrate (NO₃⁻), sulfate (SO₄²⁻), and methane sulfonic acid (MSA).

134 Furthermore, anhydro-sugars and saccharides were analysed by a High Performance Liquid Chromatography with Pulsed
 135 Amperometric Detection (HPLC-PAD), using a Thermo-Fisher ICS 5000⁺ HPLC equipped with 4 mm diameter Metrosep
 136 Carb 2×150 mm column and 50 mm pre-column in isocratic mode with 15% of an eluent of sodium hydroxide (200 mM) and
 137 sodium acetate (4 mM) and 85% water, at 1 ml min⁻¹. This method notably allowed the quantification of anhydrous saccharides

138 (levoglucosan and mannosan), polyols (arabitol and mannitol), and glucose as tracers of biomass burning and primary biogenic
139 aerosols (Samaké et al., 2019b; Waked et al., 2014).

140 Finally, major and trace elements were analysed after mineralization of a 38 mm diameter punch of each filter, using 5 ml of
141 HNO₃ (70%) and 1.25 ml of H₂O₂ during 30 minutes at 180 °C in a microwave oven (microwave MARS 6, CEM). The analysis
142 of 18 elements (Al, As, Ba, Cd, Cr, Cu, Fe, Mn, Mo, Ni, Pb, Rb, Sb, Se, Sn, Ti, V, and Zn) was performed on this extract using
143 inductively coupled plasma mass spectroscopy (ICP-MS) (ELAN 6100 DRC II PerkinElmer or NEXION PerkinElmer) in a
144 way similar to that described by (Alleman et al., 2010).

145 The procedures for filter sampling and chemical analyses have been performed following the recommendations of related EN
146 standards (i.e., EN 12341, EN 14902, EN 16909, EN 16913) (Favez et al., 2021). Moreover, quality control of the chemical
147 speciation analyses includes chemical mass closure as presented in the supplementary information (S2). It should also be
148 noted that our group successfully participates in regular inter-laboratory comparison exercises for OC and EC within ACTRIS
149 and in EMEP (European Monitoring and Evaluation Programme) for ions analysis.

150 **2.3 Additional set of analyses of organic tracers**

151 **2.3.1 Organic acids**

152 The analysis of a large array of organic acids (including pinic and phthalic acids, and 3-MBTCA) was conducted using the
153 same water extracts as for IC and HPLC-PAD analyses. In brief, this was performed by HPLC-MS (GP40 Dionex with a LCQ-
154 FLEET Thermos-Fisher ion trap), with negative mode electrospray ionization. The separation column is a Synergi 4 µm Fusion
155 – RP 80A (250×3 mm ID, 4 µm particle size, from Phenomenex). An elution gradient was optimized for the separation of the
156 compounds, with a binary solvent gradient consisting of 0.1% formic acid in acetonitrile (solvent A) and 0.1% aqueous formic
157 acid (solvent B) in various proportions during the 40-minute analytical run. Column temperature was maintained to 30 °C.
158 Eluent flow rate was 0.5 ml min⁻¹, and injection volume was 250 µl. Calibrations were performed for each analytical batch
159 with solutions of authentic standards. All standards and samples were spiked with internal standards (phthalic-3,4,5,6-d⁴ acid
160 and succinic-2,2,3,3-d⁴ acid). The calculation of the final atmospheric concentrations was corrected with the concentrations of
161 internal standards and of the procedural blanks, taking also into account the extraction efficiency varying between 76-116%
162 (depending on the acid).

163 **2.3.2 Cellulose**

164 The concentration of cellulose within PM₁₀ samples was quantified based on a protocol improving the procedure proposed by
165 Kunit and Puxbaum (1996). Cellulose was extracted from the filter in an aqueous solution, which was then processed in several
166 solutions of enzymes in order to break-down the cellulose into glucose units. Resulting glucose concentration was quantified
167 using an HPLC-PAD technique. To do so, a 21 mm diameter punch was first extracted for 40 minutes using an ultrasound bath
168 in 3 ml of an aqueous solution with thymol buffer (pH 4.8). Then two enzymes solutions (cellulase (Sigma Aldrich, C2730)

169 with 20 μl of an aqueous solution at 70 units g^{-1}) and glucosidase (Sigma Aldrich, 49291), with 60 μl of an aqueous solution
170 at 5 units g^{-1}) are added into the solution. The solution was then incubated at 50 $^{\circ}\text{C}$ for 24 hours for the hydrolysis to occur.
171 The hydrolysis is stopped by placing the solution in an oven at 100 $^{\circ}\text{C}$ for 45 minutes. The solution was then centrifuged (7000
172 rpm) for 15 minutes, and carefully extracted out using a syringe before being analysed with an HPLC-PAD instrument. The
173 procedural blanks are greatly improved when the enzymes stock solutions are filtered to lower their glucose content. This is
174 performed with a series of cleaning steps ($n=10$) by tangential ultrafiltration in a Vivaspin 15R tube at 7000 rpm in Milli-Q
175 water.

176 The HPLC-PAD (Dionex DX500) is equipped with a Metrohm column (250 mm long, 4 mm diameter), with an isocratic run
177 of 40 minutes with the eluents A (50%, 18mM NaOH), B (25%, 100 mM NaOH + 150mM NaAc), and C (25%, 220 mM
178 NaOH). Column temperature is maintained at 30 $^{\circ}\text{C}$. Eluent flow rate is 1 ml min^{-1} , and injection volume is 250 μl . Each
179 analytical batch also includes standard glucose solutions as well as standard cellulose solutions (using 20 μm beads, Sigma
180 Aldrich, S3504) that have been processed like the real samples in order to determine the specific efficiency of the cellulose-
181 to-glucose enzymatic conversion for each batch. The final calculation of the atmospheric concentration of the free cellulose
182 takes this conversion efficiency into account. It varied according to the batch, generally ranging from 65–80%. The calculation
183 of the cellulose concentration also takes into account the initial concentrations of atmospheric glucose of each sample,
184 determined in parallel with the HPLC-PAD analysis of sugars and polyols as described above. Finally, field and procedural
185 blanks are also taken into account.

186 **2.4 Source apportionment**

187 **2.4.1 PMF input dataset**

188 Source apportionment of PM_{10} was conducted using the United States Environmental Protection Agency (US-EPA) software
189 PMF 5.0 (Norris et al., 2014), aiming at the identification and quantification of the major sources of PM_{10} for the three urban
190 sites in the Grenoble basin. Briefly, PMF is based on the factor analysis technique (Paatero and Tapper, 1994) applying a
191 weighted least-squares fit algorithm allowing the resolution of Eq. S1 (see supplementary information (SI)). In our study, 35
192 chemical species were used as input variables, namely OC^* , EC, ions (Na^+ , K^+ , NH_4^+ , Mg^{2+} , Ca^{2+} , NO_3^- , SO_4^{2-} and Cl^-), trace
193 metals (Al, As, Cd, Cr, Cu, Fe, Mn, Mo, Ni, Pb, Rb, Sb, Se, Sn, Ti, V and Zn) and organic tracers (MSA, levoglucosan,
194 mannosan, polyols (sum of arabitol and mannitol), pinic acid, 3-MBTCA, phthalic acid, and cellulose), as summarized in Table
195 S1 in SI. We assumed that arabitol and mannitol originated from the same source, and hence combined them into one
196 component labelled as “polyols” (Samaké et al., 2019a). In order to avoid double counting of carbon mass, OC^* was calculated
197 as the difference between total OC and the quantity of C atoms contained in the different organic markers included in the PMF
198 input data matrix (as detailed in Eq. S2). The uncertainties of the input variables were calculated using Eq. S3 (Gianini et al.,
199 2012). Finally, the species displaying a signal-to-noise ratio (S/N) lower than 0.2 were discarded and those with S/N between
200 0.2 and 2 were classified as “weak” variables (and then down-weighted applying 3-fold uncertainties).

201 **2.4.2 Set of constraints**

202 Since mixing issues between factors are inherent to PMF (i.e., collinearity due to meteorological conditions) and to possible
 203 rotational ambiguity in the solution, we applied a set of constraints to the selected best base case solutions thanks to the ME-2
 204 solver (Paatero, 1999). The constraints used were similar to that of Weber et al. (2019), who applied a minimum set of
 205 constraints to a large series of data sets within the SOURCE program. We also added specific constraints for the traffic factor,
 206 derived from a previous study in Grenoble dedicated to traffic emissions (Charron et al., 2019), as summarized in Table 1.
 207 These constraints were applied similarly to the data sets from the 3 sites. This allows the orientation of the PMF solution
 208 towards more stable and environmentally realistic profiles.

209
 210 **Table 1: Summary of the applied chemical constraints on source-specific tracers in the PMF factor profiles.**

Factor profile	Element	Type	Value
Biomass burning	Levoglucosan	Pull up maximally	(% dQ 0.50)
Biomass burning	Mannosan	Pull up maximally	(% dQ 0.50)
Primary biogenic	Levoglucosan	Set to zero	0
Primary biogenic	Mannosan	Set to zero	0
Primary biogenic	Polyols	Pull up maximally	(% dQ 0.50)
Primary biogenic	EC	Pull down maximally	(% dQ 0.50)
MSA-rich	MSA	Pull up maximally	(% dQ 0.50)
MSA-rich	Levoglucosan	Set to zero	0
MSA-rich	Mannosan	Set to zero	0
MSA-rich	Polyols	Pull down maximally	(% dQ 0.50)
MSA-rich	EC	Pull down maximally	(% dQ 0.50)
Nitrate-rich	Levoglucosan	Set to zero	0
Nitrate-rich	Mannosan	Set to zero	0
Mineral dust	Ti	Pull up maximally	(% dQ 0.50)
Primary traffic	Levoglucosan	Set to 0	0
Primary traffic	Mannosan	Set to 0	0
Primary traffic*	Cu	Pull up maximally	(% dQ 0.50)
Primary traffic*	Fe	Pull up maximally	(% dQ 0.50)
Primary traffic*	Sn	Pull up maximally	(% dQ 0.50)
Primary traffic*	Ca ²⁺	Pull down maximally	(% dQ 0.50)
Primary traffic	Cu/Fe	Set to value	0.046 (% dQ 0.50)
Primary traffic	Cu/Sn	Set to value	5.6 (% dQ 0.50)
Primary traffic	Cu/Sb	Set to value	12.6 (% dQ 0.50)
Primary traffic	Cu/Mn	Set to value	5.7 (% dQ 0.50)
Primary traffic	OC*/EC	Set to value	0.44 (% dQ 0.50)

211 Note: *Only applied in Vif (peri-urban) site

212 2.4.3 Criteria for a valid solution

213 Solutions with a total number of factors between 7 and 12 were tested for the determination of the base cases. During factor
214 selection, the Q/Q_{exp} ratio (<1.5), the geochemical interpretation of the factors, the weighted residual distribution, and the total
215 reconstructed mass were evaluated. Finally, the optimal solutions obtained for each urban site was subjected to error estimation
216 to ensure stability and accuracy of the solutions, using displacement (DISP) and bootstrapping (BS) methods. The DISP
217 analysis evaluates that no swapping had occurred in any of the factors. Solutions with >80 out of 100 BS mapped factors were
218 considered appropriate solutions. The final retained optimal solutions after the application of constraints fulfilled the
219 recommendations of the European guide on air pollution source apportionment with receptor models (Belis et al., 2014). The
220 sensitivity of the solutions to the applied constraints was also carefully evaluated by comparison between the base and
221 constrained cases. More information about the source apportionment methodology is provided in the SI.

222 2.4.4 Similarity assessment

223 A test of similarity between source profiles, based on their specific chemical relative mass composition at each site, was
224 performed by comparing the Pearson distance (PD) and standardized identity distance (SID). This allows the evaluation of the
225 variability of the solutions across these different urban environments. The PD and SID were calculated using Eq. S4 (Belis et
226 al., 2015).

227 The PD metric represents the sensitivity of a chemical profile based on the differences in the major mass fractions of PM,
228 whereas the SID represents the sensitivity to all components (hence taking into account trace species). Homogenous profiles
229 that are stable over different site types are expected to have $PD < 0.4$ and $SID < 1.0$ (Pernigotti and Belis, 2018). Conversely,
230 factors outside of this range are considered to have heterogeneous profiles.

231

232 2.4.5 Estimation of the contribution uncertainties

233 The BS profiles uncertainties for the obtained solutions are presented in the SI (S3), in the form of $mean \pm std$ of the 100 BS for
234 all sites. As PMF5.0 does not directly output this to the user, we provided an estimate of the contribution uncertainties based
235 on the method presented in Weber et al. (2019). During the BS estimation, both the G and F matrices are available, however
236 only the F matrix is given back to the user (the G matrix being used internally to map the different profiles). Hence, the daily
237 contributions of each of the species are estimated using:

$$238 X_{BSi} = G_{ref} \times F_{BSi}$$

239 where F_{BSi} is the profile of the bootstrap i , and X_{BSi} is the time series of each species according the reference contribution G_{ref}
240 and the bootstrap run F_{BSi} . Similarly, the DISP contribution uncertainties are given by the reference contribution G multiplied
241 by the lower and upper limits of the DISP result for each species.

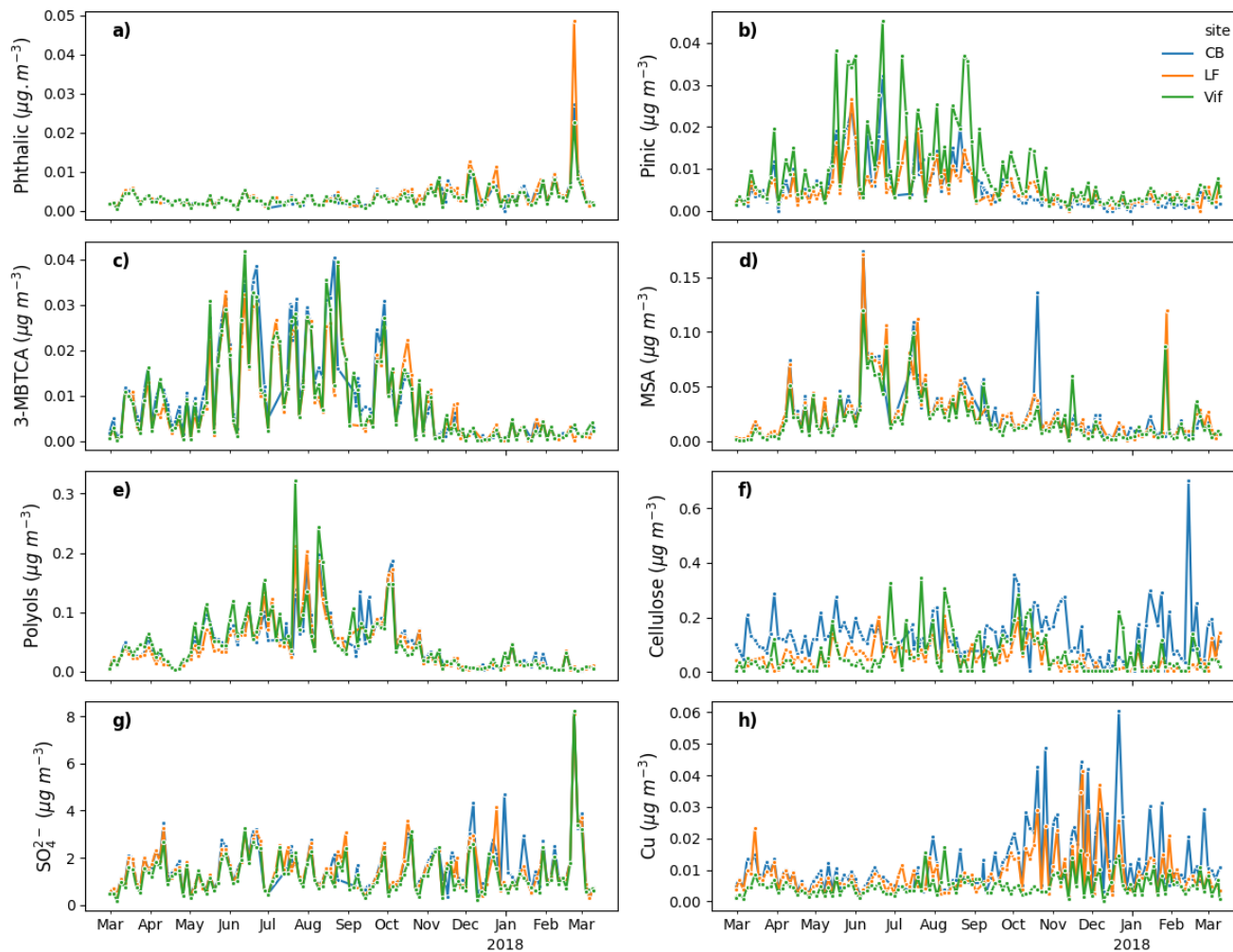
242 3 Results and discussion

243 3.1 General evolution of concentrations of PM₁₀ and chemical species

244 The daily PM₁₀ mass concentrations at the three measurement sites, determined with the TEOM-FDMS for the dates of filter
245 sampling, ranged from 3-61 $\mu\text{g m}^{-3}$ with an overall average of $14\pm 9 \mu\text{g m}^{-3}$ during the sampling period. Average PM₁₀ levels
246 were the highest at the urban hyper-center site (CB) ($16\pm 10 \mu\text{g m}^{-3}$), followed by the urban background site (LF) ($14\pm 8 \mu\text{g m}^{-3}$),
247 and the peri-urban site (Vif) ($13\pm 9 \mu\text{g m}^{-3}$). Annual averages of PM₁₀ mass concentrations and chemical compositions at all
248 sites and at individual urban sites are shown in Table S2 in SI. The sites in this study showed minimal exceedances of the
249 current PM₁₀ European limit value of $40 \mu\text{g m}^{-3}$ (3.7%, 1.6%, and 1.6% of measurement days at the LF, CB, and Vif sites,
250 respectively). Most of these exceedances occurred during the winter season indicating the necessity to additionally implement
251 season-specific regulations for PM₁₀ emission reductions. Organic matter (OM) was the largest contributor in PM₁₀ and
252 accounted for 54%, 51%, and 56% of mass concentration on an annual basis in LF, CB, and Vif, respectively. This was
253 followed by contributions from the major inorganic species (NH_4^+ , NO_3^- , and SO_4^{2-}), suggesting strong influence from
254 secondary inorganic aerosol (SIA) that are generally associated with long-range transport of pollutants or the occurrence of a
255 small scale thermal inversion within the Grenoble basin. An extensive description of the PM₁₀ chemistry in the Grenoble basin
256 has already been presented in Srivastava et al. (2018b) for the years 2013–2014 at the LF site. Our results showed notable
257 similarities for most chemical species for the year 2017–2018, especially in terms of seasonal variations and respective
258 contribution of chemical species to PM₁₀ mass concentrations. Therefore, we will only describe these aspects briefly in this
259 paper.

260 First, the time series analysis of PM₁₀ and its chemical composition in the Grenoble basin during the sampling period showed
261 mild to strong seasonal trends. Part of it can be attributed to the atmospheric dynamics in the area given its alpine environment
262 resulting in atmospheric temperature inversions that are especially common in winter. In the absence of strong winds during
263 the winter season (especially during anti-cyclonic periods), higher concentrations of air pollutants could be expected. Indeed,
264 PM₁₀ concentrations were higher during the colder months (October to April) with an average of $17\pm 10 \mu\text{g m}^{-3}$ and lower
265 during the warmer months (May to September) with an average of $10\pm 4 \mu\text{g m}^{-3}$.

266



267

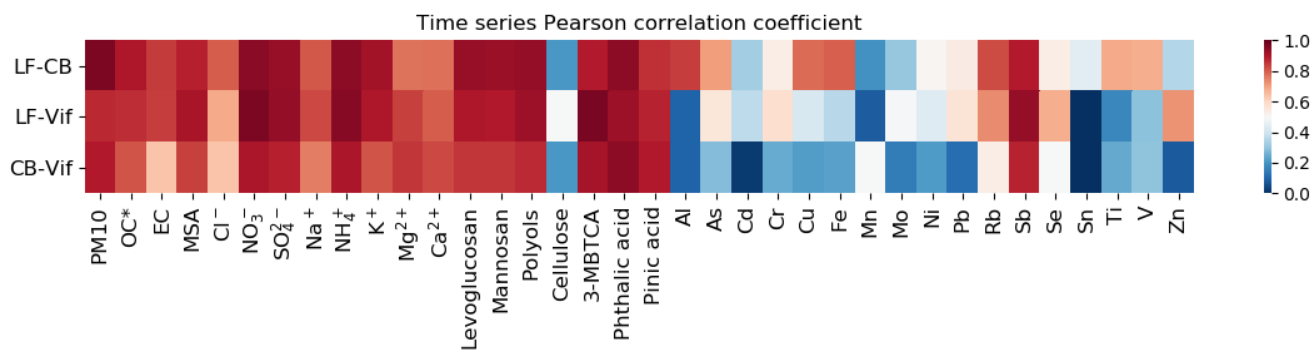
268 **Figure 2: Temporal evolutions of a) phthalic acid, b) pinic acid, c) 3-MBTCA, d) MSA, e) polyols (arabitol+mannitol), f) cellulose,**
 269 **g) SO_4^{2-} and h) Cu in the three urban sites in the Grenoble basin (LF in orange, CB in blue, and Vif in green).**

270

271 We observed a strong seasonality for some chemical species with higher concentrations during the colder months including
 272 OC^* , EC, K^+ , NO_3^- , NH_4^+ , levoglucosan, mannosan, and phthalic acid. These species are commonly associated with primary
 273 emissions during the process of biomass burning (OC , EC, K^+ , levoglucosan, mannosan) and secondary atmospheric
 274 processing (NO_3^- , NH_4^+ , phthalic acid). Alternatively, specific species with higher concentrations during warmer months
 275 include MSA, polyols, 3-MBTCA, and pinic acid. These species are known to be products of a wide range of photochemical
 276 reactions in the atmosphere partly formed by OH-initiated oxidation (Atkinson and Arey, 1998; Szmigielski et al., 2007) and
 277 can be explained by enhanced photochemical production due to an increase of temperature-dependent hydroxyl radical (OH)

278 concentration. A summary of temporal evolutions of the concentration for some species including SO_4^{2-} , Cu, cellulose, polyols,
 279 3-MBTCA, pinic acid, and phthalic acid is shown in Figure 2.

280 Second, the Pearson correlation coefficients of the temporal evolution of each specie across sites is presented in Figure 3.
 281 Similarity of temporal trends and strong correlations of PM_{10} components between our 3 sites indicates the influence of large
 282 scale transport processes or possible uniform distribution of some emission sources in the Grenoble area. Further, the
 283 accumulation and removal processes of the PM may be driven by similar season-specific environmental conditions at a local
 284 scale. A strong correlation was observed in OC^* , EC, ions, polyols, levoglucosan, mannosan, 3-MBTCA, phthalic acid, and
 285 pinic acid between sites suggesting similar origins and atmospheric processes affecting the concentrations of these species.
 286 The three sites seem to be equally impacted by long range transport since concentration of SO_4^{2-} appears almost identical. We
 287 also clearly see relatively similar temporal trends for the organic acids (MSA, pinic, and 3-MBTCA). Notably, we also
 288 observed an important episode in phthalic acid in late February 2018 affecting all the three sites. An extensive discussion on
 289 the formation processes of anthropogenic SOA in high concentration events was already provided in Srivastava et al. (2018b).
 290 However, this new observation brings in the hypothesis that these processes may take place specifically due to heterogeneous
 291 chemistry when associated with fog episodes, as it can be observed by local web cams over the city (discussed in answers to
 292 reviewers). Conversely, cellulose and most metal species showed weak to mild correlations between sites, possibly indicating
 293 that the sources of these species are highly localized, with a potential impact that is variable at a city-scale. Particularly,
 294 cellulose presents similar order of magnitude at the three sites but presents higher concentration at CB, especially during
 295 winter. A few metals only showed strong correlations between LF and CB, but not with Vif, such as Al, Cu, Fe, Rb, and Sb
 296 which are tracers of road transport activity or biomass burning emissions. Specifically, Cu concentrations are similar at the
 297 three sites during summer, but presents significantly lower concentration in Vif compared to the two urban sites of CB and LF
 298 during winter.



300
 301 **Figure 3: Concentration time series Pearson correlation coefficient of PM_{10} and its chemical composition between LF and CB (LF-**
 302 **CB), LF and Vif (LF-Vif), and CB and Vif (CB-Vif).**

303

304 **3.2 PM₁₀ source apportionment**

305 In the following sections, a description of the best PMF solution obtained after application of constraints is provided for each
306 of the 3 sites, together with a discussion about the factors that are associated with the added organic tracers (MSA, polyols,
307 cellulose, pinic and 3-MBTCA acids). The presentation of error estimations, chemical profiles, and temporal evolutions of the
308 PMF-resolved sources, and the discussion about the more classical factors can be found in the SI (S3).

309 **3.2.1 General description of the solutions**

310 The PMF model was applied independently on the data set of each three sites, using 35 chemical atmospheric compounds in
311 each site. The constrained solutions for each site consist of 11 factors, including common factors such as primary traffic,
312 biomass burning, nitrate-rich, sulfate-rich, aged sea salt, sea/road salt, and mineral dust. Also, with the use of biogenic tracer
313 species, we identified a primary biogenic factor and a MSA-rich factor. These factors are similarly determined in Weber et al.
314 (2019) for each of 15 sites in France. We also determined a metals-rich factor, identified as an industrial factor, accounting for
315 a very small part of the PM₁₀ mass. Finally, using new organic proxies (pinic and 3-MBTCA acids), we identified a secondary
316 biogenic oxidation factor that is rarely described in other PMF studies. Table 2 shows a synthesis of the tracers used to identify
317 these 11 PMF-resolved factors that are found at each of the 3 sites.

318 Other solutions with fewer or greater number of factors were also investigated but these solutions were less defined, and factor
319 merging was often observed. The reconstructed PM₁₀ contributions from all sources with measured PM₁₀ concentration showed
320 very good mass closure in all sites (LF: $r=0.99$, $n=125$, $p<0.05$; CB: $r=0.99$, $n=126$, $p<0.05$; and Vif: $r=0.99$, $n=126$, $p<0.05$)
321 indicating very good model results.

322 This result is in line with a previous study in the city of Grenoble (Srivastava et al., 2018b), but with slight improvements in
323 the PM₁₀ mass closure (from $r=0.93$ to $r=0.99$). A complete comparison of the PMF-resolved sources between the two studies
324 is presented and discussed in SI (S4). The two sets of results are in good agreement, despite the samples being collected 4
325 years apart. There were several identified sources that are similar in both studies such as biomass burning, primary traffic,
326 mineral dust, aged sea salt, sulfate- and nitrate-rich (identified collectively as secondary inorganics in Srivastava et al. (2018b)),
327 and primary biogenic (identified as fungal spores and plant debris in Srivastava et al. (2018b)). Additionally, due to a number
328 of differences in the input variables used, there are some sources that are completely unique to each study. In particular, the
329 sources that we have uniquely identified are industrial, sea/road salt, MSA-rich, and secondary biogenic oxidation sources.
330 Conversely, Srivastava et al. (2018b) have uniquely identified two SOA sources: biogenic SOA and anthropogenic SOA. It
331 can be argued that the secondary biogenic oxidation source (11%) in our study and the biogenic SOA (12%) in Srivastava et
332 al. (2018b) are in some way similar, although different tracers were used to identify them. Particularly, Srivastava et al. (2018b)
333 identified the biogenic SOA source with high contributions from α -methylglyceric acid (α -MGA and 2-methylerythritol (2-
334 MT) that are isoprene oxidation products and hydroxyglutaric acid (3-HGA), an oxidation product from α -pinene. On the other

335 hand, our study identified the secondary biogenic oxidation source with high contributions from 3-MBTCA and pinic acid
 336 (essentially from α -pinene oxidation). While not uniquely identified in our study, the contributions of phthalic acid in several
 337 common anthropogenic-derived sources (sulfate- and nitrate-rich) can also mark the potential contributions from
 338 anthropogenic SOA sources. Finally, the considerable economic advantage in the specific organic tracers used in our study, in
 339 terms of the type of chemical analyses performed, could assist future studies utilizing organic species in PMF.

340 It is also important to note that, although still in the acceptable range, the sulfate-rich factor obtained in our PMF results yielded
 341 the most BS unmapped factors amongst the PMF-resolved factors (up to 25% for the CB site). This may be the sign of possible
 342 mixing of different processes / sources in this factor.

343

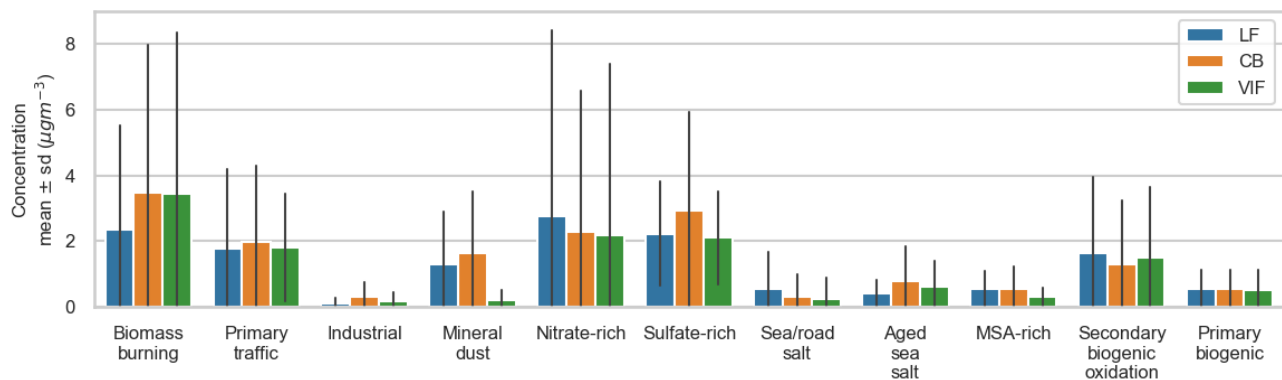
344 **Table 2: Summary of PMF-resolved sources and their specific tracers.**

Identified factors	Specific tracers
Biomass burning	Levoglucosan, mannosan, K ⁺ , Rb, Cl ⁻
Primary traffic	EC, Ca ²⁺ , Cu, Fe, Sb, Sn
Nitrate-rich	NO ₃ ⁻ , NH ₄ ⁺
Sulfate-rich	SO ₄ ²⁻ , NH ₄ ⁺ , Se
Mineral dust	Ca ^{2+*} , Al, Ti, V
Sea/road salt	Na ⁺ , Cl ⁻
Aged sea salt	Na ⁺ , Mg ²⁺
Industrial	As, Cd, Cr, Mn, Mo, Ni, Pb, Zn
Primary biogenic	Polyols, cellulose
MSA-rich	MSA
Secondary biogenic oxidation	3-MBTCA, pinic acid

345 Note: *Vif site did not have high loadings of Ca²⁺ specie in this factor

346 3.2.2 PM₁₀ contribution

347 Biomass burning (17-26%), sulfate-rich (16-18%), and nitrate-rich (14-17%) sources were the highest contributors to the total
 348 PM₁₀ mass on a yearly average in the Grenoble basin. Primary traffic (12-14%) and secondary biogenic oxidation (8-11%)
 349 sources also contributed a relevant amount. Figure 4 presents a comparison of the source contributions in each site based on
 350 mass concentration (in $\mu\text{g m}^{-3}$). These results are in line with recent studies leading to anthropogenic and SOA sources heavily
 351 influencing urban air pollution in western Europe (Daellenbach et al., 2019; Golly et al., 2019; Pandolfi et al., 2020; Srivastava
 352 et al., 2018b; Weber et al., 2019). The most notable difference across all sites is the sharp decrease of mineral dust in Vif
 353 compared to the other two urban sites, and this is discussed further in section 3.4.1.



354

355 **Figure 4: Factor contributions in $\mu\text{g m}^{-3}$ for the three sites (LF: blue, CB: orange, Vif: green). Bar plots depict the mean annual**
 356 **value and the standard deviation of daily variations.**

357

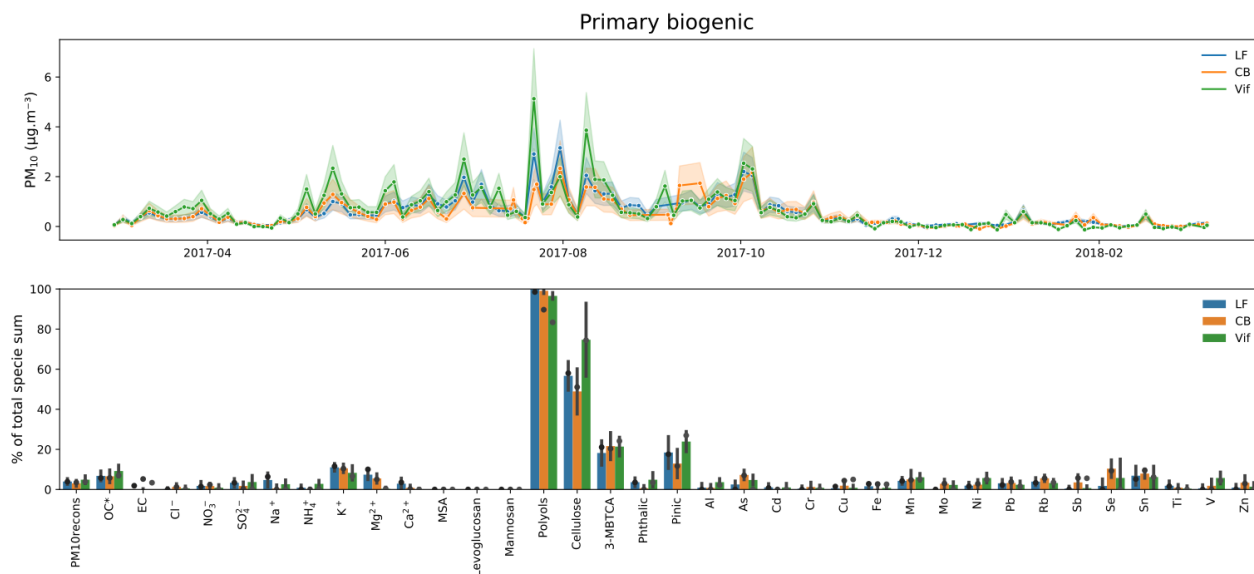
358 3.2.3 MSA-rich

359 This factor is identified with a high loading of MSA, a known product of oxidation of dimethylsulfide (DMS), commonly
 360 described as resulting from marine phytoplankton emissions (Chen et al., 2018; Li et al., 1993). Other chemical species with
 361 significant concentrations in this factor include sulfate and ammonium. Although a very useful tracer of marine biogenic
 362 sources, MSA showed in our series only weak to mild correlations with ionic species from marine aerosols such as Na^+ (r:
 363 0.2–0.3) and Mg^{2+} (r: 0.3–0.4). This suggests potential emissions originating from terrestrial biogenic sources instead, which
 364 has been similarly suggested before (Bozzetti et al., 2017; Golly et al., 2019), and/or from forest biota (Jardine et al., 2015;
 365 Miyazaki et al., 2012). On an annual scale, this factor accounted for 2–4% of the total mass of PM_{10} and shows a strong
 366 seasonality with highest contributions during summer, reaching up to 53%, 57%, 52% of the total PM_{10} mass in some specific
 367 days in LF, CB, and Vif, respectively. The similarity in the temporal distribution across sites, as shown in Figure S3.8,
 368 especially the summer peaks, could be linked to the influence of long-range transport of pollutants in the MSA-rich factor.

369 3.2.4 Primary biogenic

370 The primary biogenic factor was identified with high loadings of both polyols and cellulose (see Figure 5). Polyols (represented
 371 by the sum of arabitol and mannitol) are known as tracers of primary biological aerosols from fungal spores and microbes
 372 (Bauer et al., 2002; Igarashi et al., 2019). Polyols has been used in several studies as a tracer of biogenic sources, contributing
 373 in France within a range of 5–9% of PM_{10} on a yearly average (Samaké et al., 2019b; Srivastava et al., 2018b; Waked et al.,
 374 2014; Weber et al., 2019). Cellulose is a potential macro-tracer for plant debris from leaf litter and seed production (Kunit and
 375 Puxbaum, 1996; Puxbaum, 2003) that is very rarely used in source apportionment studies as of today. It can represent a large

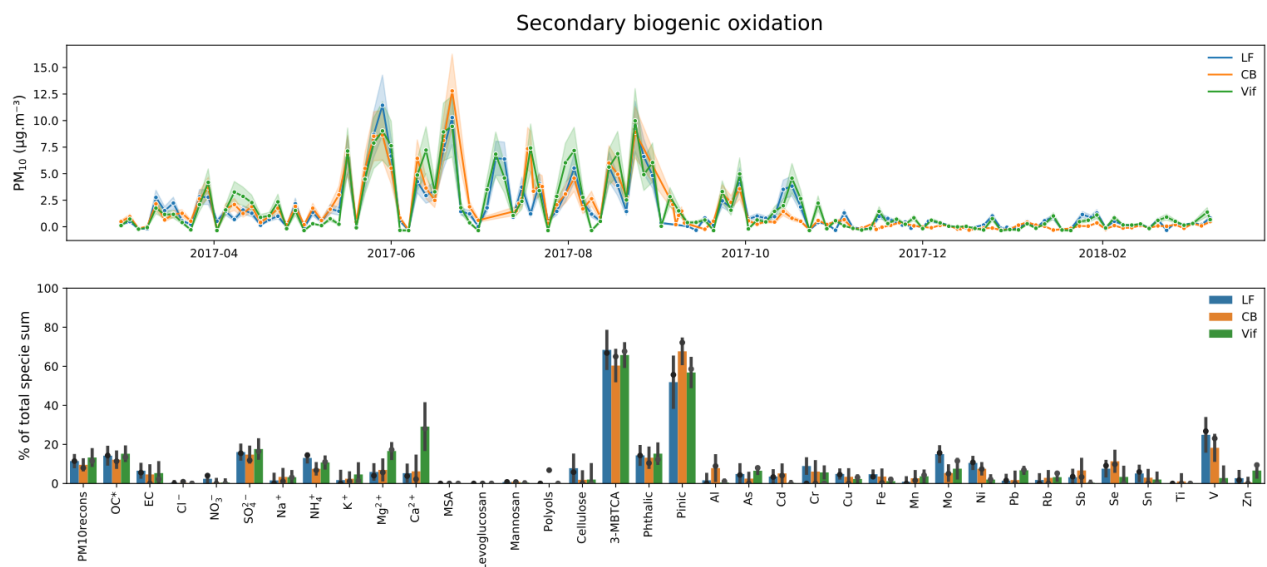
376 fraction of the PM mass in the coarse mode (Bozzetti et al., 2016) and it represents up to 6% during the warm season in the
 377 Vif site.
 378



379
 380 **Figure 5: Primary biogenic factor for the 3 urban sites. Top: Contribution to PM₁₀ given the mean and standard deviation of the**
 381 **100 BS. Bottom: Percentage (%) of each specie apportioned by this factor (dots refer to the constrained run, bar plots refer to the**
 382 **mean and error bars refer to the standard deviation of the 100 BS).**

383
 384 A strong correlation was found in the temporal evolution of polyols across the 3 sites in our study indicative of large scale
 385 impact of sources for these species (Samaké et al., 2019b). Conversely, cellulose concentrations present only weak correlations
 386 across the 3 sites, possibly indicating that the influence of the sources of this specie might be more local. Although polyols
 387 and cellulose are both tracers of primary biogenic sources, only a rather mild correlation ($r=0.5$) was found between these two
 388 tracers, with seasonality of their concentrations being slightly different (Figure 2). It shows that the processes and the sources
 389 are probably distinct for the two sets of chemical species. However, the PMF is not able to separate them, and this factor
 390 includes most of the cellulose (58, 51, and 74 % in LF, CB, and Vif, respectively), and also most of the polyols (99, 90, and
 391 83 % in LF, CB, and Vif, respectively). The remaining fraction of cellulose concentrations was included in the mineral dust
 392 factor in LF and CB, and in the primary traffic factor in Vif, suggesting the possibility of resuspension processes for this
 393 compound (see the SI for details). We can also note that the cellulose was not at all apportioned in the biomass burning factor,
 394 an indication that it may not be emitted by this source.
 395 Despite their slightly different origins, the PMF analysis captures the combined contribution of polyols and cellulose to a factor
 396 that can be termed “primary biogenic sources”. In this study, this factor accounted for 3-4% of the total mass of PM₁₀ on an
 397 annual scale, and a strong seasonality was observed, with up to 18% (in LF), 8% (in CB), and 17% (in Vif) of the total PM₁₀

398 mass on average in summer, with specific days reaching up to 60% of PM_{10} for example at the Vif site (see Figure 5). These
 399 temporal variations are consistent with higher biological activity (increased production of fungal and fern spores, and pollen
 400 grains) in this season due to increase in temperature and humidity (Graham et al., 2003; Verma et al., 2018). This may also be
 401 attributed to an increased plant metabolic activity (production of plant debris from decomposition of leaves) and the proximity
 402 to forested and agricultural areas of the sampling sites (Gelencsér et al., 2007; Puxbaum, 2003). Finally, one can note that the
 403 chemical profiles also include some fractions of the tracers from secondary biogenic production (3-MBTCA and pinic acid),
 404 indicative of some degree of mixing between primary and secondary biogenics.
 405



406
 407 **Figure 6: Secondary biogenic oxidation factor for the 3 urban sites. Top: Contribution to PM_{10} given the mean and standard**
 408 **deviation of the 100 BS. Bottom: Percentage (%) of each specie apportioned by this factor (dots refer to the constrained run, bar**
 409 **plots refer to the mean and error bars refer to the standard deviation of the 100 BS).**

410

411 3.2.5 Secondary biogenic oxidation

412 The secondary biogenic oxidation factor was identified with high loadings of 3-MBTCA and pinic acids (see Figure 6). Both
 413 tracers of this factor are known to be products of secondary oxidation processes of alpha-pinene from various biogenic origins.
 414 As suggested by the nearly identical mass fraction determined in Srivastava et al., (2018) at the same site, this factor may as
 415 well contain some PM resulting from the oxidation of isoprene epoxydiols (IEPOX) (Surratt et al., 2010; Zhang et al., 2017)
 416 that may present a rather similar seasonality (Budisulistiorini et al., 2013, 2016), but this is still an open question.

417 The apportionment of such a factor is not commonly achieved in receptor modelling using off-line tracers (van Drooge and
 418 Grimalt, 2015; Heo et al., 2013; Hu et al., 2010; Srivastava et al., 2018a). On an annual scale in our study, this factor accounted

419 for 8-11% of the total mass of PM₁₀, but can be as high as 58% (11 µg m⁻³) on specific days (see Figure 6, Top). The strong
420 correlation between 3-MBTCA and pinic acids suggests similarity of origin of the secondary biogenic oxidation factor in the
421 Grenoble area, despite inter-site correlations for 3-MBTCA (older oxidation state of alpha-pinene, hence more homogeneous
422 at the city scale) being larger than that for pinic acid (former oxidation product, less homogeneous). Although significant
423 portions (56-72%) of these species (3-MBTCA and pinic acids) are in this secondary biogenic oxidation factor, there are still
424 relevant contributions in other factors, including primary biogenic, sulfate- and nitrate-rich, aged sea salt, and MSA-rich.
425 Conversely, the presence of phthalic acid contribution in this factor (around 10% of its concentration), which could be emitted
426 directly from biomass burning or formed during secondary processing from anthropogenic emissions (Hyder et al., 2012;
427 Kleindienst et al., 2007; Wang et al., 2017b; Yang et al., 2016), also suggests that this factor has anthropogenic influence. All
428 of these indicate that the PMF process did not deliver a pure secondary biogenic oxidation factor, either due to data processing
429 limitation or because of real mixing of these sources in the PM.

430

431 **3.3 Re-assignment of factors thanks to the new proxies**

432 **3.3.1 Importance of the new proxy for factor identification**

433 With the use of these additional organic tracers, there are several added information drawn from the results of the PMF model.
434 First, the notable contributions of phthalic acid in several sources could further confirm the mixing influence of anthropogenic
435 processes in various sources of PM₁₀ such as sulfate- and nitrate-rich, but also with secondary biogenic oxidation sources.
436 Second, adding 3-MBTCA and pinic acids in the input variables allowed the identification of a significant secondary biogenic
437 oxidation factor that is generally difficult to identify with PMF studies of off-line samples. Comparisons already started with
438 the factors obtained by AMS studies (Vlachou et al., 2018), but more work remain to be done in order to evaluate their proper
439 correspondence.

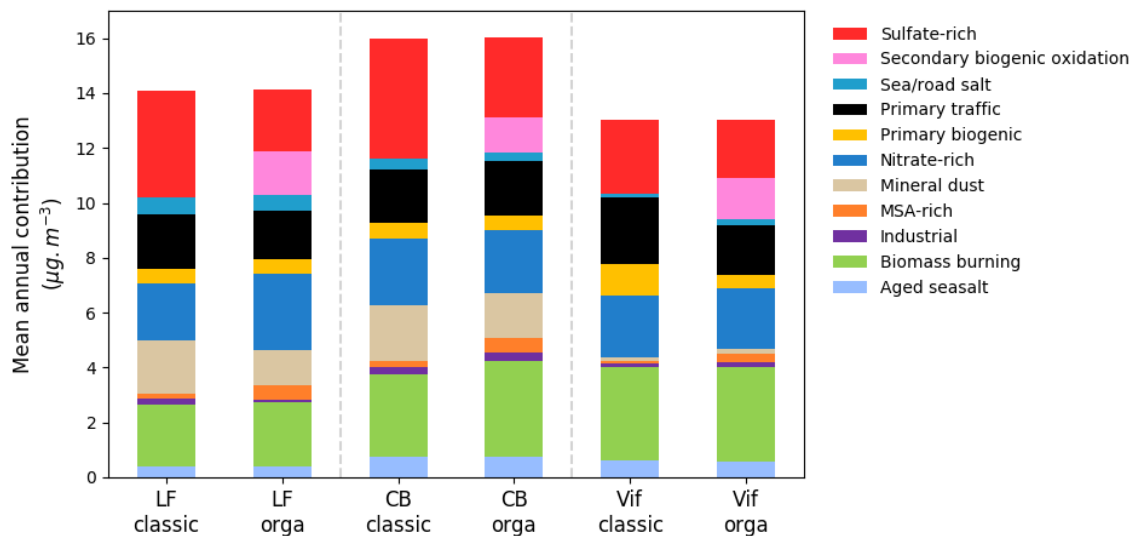
440 **3.3.2 Comparison with a “classic” PMF solution**

441 In order to quantify the added value and the changes brought in by the additional tracers, a reference PMF using a chemical
442 dataset (not including cellulose, pinic acid, phthalic acid, and 3-MBTCA) and parameters similar to that in the SOURCES
443 project (Weber et al., 2019) was performed, hereafter called “classic”, and the results were compared with those from the
444 present study (called “orga”). Figure 7 shows the comparison of the yearly average mass contribution of the different factors
445 for these two approaches. A detailed comparison of chemical profiles between the “classic” and “orga” PMF runs in each site
446 is summarized in the SI (S3). One can see that most observations below are consistent in all three sites.

447 Some factors remain unaffected or only marginally modified: it is the case for the biomass burning source with a percentage
448 increase in contribution, only ranging from 1-14%, in the “orga” compared to the “classic” PMF run across all sites. The
449 primary biogenic source also posed an interesting case with a minimal decrease in contribution at 0.1 and 6% in the LF and
450 CB sites, respectively. However, adding more specific biogenic tracers changed the contribution of the primary biogenic factor

451 in Vif, from $1.1 \mu\text{g m}^{-3}$ for the “classic” PMF down to $0.50 \mu\text{g m}^{-3}$ for the “orga” PMF run, a value that is much more in line
 452 with the contributions observed at the other sites (0.56 and $0.55 \mu\text{g m}^{-3}$ in CB and LF, respectively). This further highlights
 453 the usefulness of the additional organic tracers (e.g., addition of cellulose in the primary biogenic factor), especially for specific
 454 site typologies.

455 Conversely, the most impacted factor is the sulfate-rich one, to a similar extent for the 3 sites with much higher mass fraction
 456 in the “classic” PMF run in large part due to higher loadings of OC*. It may indicate possible merging with organic aerosol
 457 sources in the “classic” PMF, as presented in a comparison of chemical profiles between the “classic” and “orga” PMF runs
 458 in each site summarized in the SI (S3). Figure 7 shows that the differences are really close to the content of the new secondary
 459 biogenic oxidation factor. Secondary aerosols, such as the sulfate-rich factor, can be transported over long distances and can
 460 remain in the atmosphere for about a week (Warneck, 2000), allowing them to interact with numerous other species and
 461 undergo different atmospheric oxidation processes. In fact, several studies have investigated various oxidation pathways of
 462 sulfate-rich sources (Barker et al., 2019; Ishizuka et al., 2000; Schneider et al., 2001; Ullerstam et al., 2002, 2003; Usher et al.,
 463 2002). In the SPECIEUROPE database, several studies have reported sulfate-rich sources influenced by a variety of different
 464 fuel combustion sources (Bove et al., 2014; Pernigotti et al., 2016; Pey et al., 2013). It is, therefore, not surprising that part of
 465 the matter in the sulfate-rich source was re-assigned to different other sources upon addition of the organic tracers in the “orga”
 466 PMF run. A comparable study in Metz (France) also used another organic tracer (oxalate) to apportion a secondary organic
 467 aerosol (SOA) source from PM, ascribing it possibly to both biogenic and anthropogenic emissions (Petit et al., 2019).
 468



469 **Figure 7: Mean annual contribution ($\mu\text{g m}^{-3}$) of PMF-resolved factors of PM₁₀ in the Grenoble basin using a classic set of input**
 470 **variables similar to SOURCES (“classic”) and using additional new organic tracers (“orga”).**
 471

472

473 We also observed an increase in the contributions of the MSA-rich factor at the three sites, with an increase in contributions
474 from specific inorganic species, such as SO_4^{2-} and NH_4^+ (see Figure S3.8.1 in the SI). Conversely, a decrease in contribution
475 from polyols was observed in the chemical profile of primary biogenic factor in Vif (see Figure S3.7.1 in the SI). Results show
476 that in the “classic” PMF run, the contribution of polyols was almost completely assigned to the primary biogenic factor (>94%
477 of its total mass). On the other hand, the “orga” PMF run resulted in a contribution of polyols to the MSA-rich factor of about
478 10% of its total mass.

479 Finally, there is also an observed re-assignment of the Ca^{2+} specie that further refined specific factors in Vif. The mineral dust
480 factor is often identified with high loadings of Ca^{2+} , however this is not the case for Vif, particularly for the “classic” PMF run
481 (less than 1% of total Ca^{2+} , although attached with important uncertainties). It is important to note that Ca^{2+} in an urban
482 environment can come from several sources such as construction activities and global resuspended dust from various activities
483 (from biomass burning and traffic). Previous studies comparing measurements at LF and a site close to a highway (2 km apart)
484 showed a 34% increment of this factor near the highway, supporting the influence of resuspended dust with traffic (Charron
485 et al., 2019). With the addition of the organic tracers, there was an observed increase in the contribution of Ca^{2+} in the mineral
486 dust factor in Vif (see Figure S3.11.1), resulting to more than 20% of the total Ca^{2+} apportioned in this factor (a value is still
487 attached with important uncertainties). Interestingly, the contribution of Ca^{2+} is mainly transferred from the primary traffic
488 factor to the mineral dust factor. This resulted to a decreased contribution of the primary traffic factor in Vif from $2.4 \mu\text{g m}^{-3}$
489 for the “classic” PMF down to $1.8 \mu\text{g m}^{-3}$ for the “orga” PMF run. Again, this is a value closer to the contributions at the other
490 sites (2.0 and $1.8 \mu\text{g m}^{-3}$ in CB and LF, respectively) (see Figure S3.2.1 in the SI).

491 **3.3.3 Decrease of uncertainties**

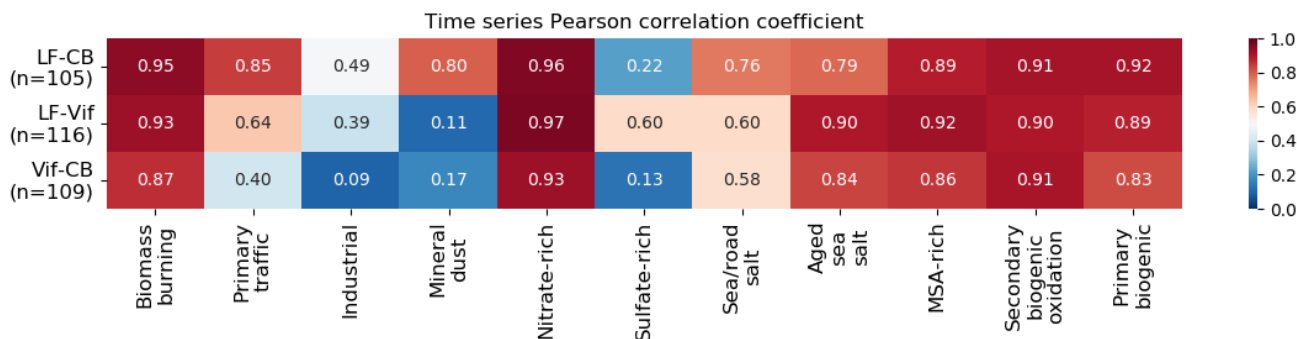
492 Another advantage of adding specific proxies in the PMF is the lowering of uncertainties associated with some other chemical
493 species in some factors. Indeed, we observed a decrease of the BS uncertainties, notably for the OC* and also for some main
494 tracers of sources in several profiles (see in the SI (S3)). The sulfate-rich is the most impacted factor when adding the new
495 organic tracers and the higher uncertainties in the “classic” PMF run provided insights that this profile may have some internal
496 mixing. Splitting this factor, thanks to the new organics, refined the sulfate-rich factor and strengthened the BS stability of this
497 factor, decreasing the BS uncertainties.

498 Concerning the DISP, the range of uncertainties was also narrowed for 74% of the species in factors when comparing the
499 “classic” and “orga” PMF. This decrease of uncertainties for the DISP when adding new variables was already observed by
500 (Emami and Hopke, 2017), but our study additionally observed this in the BS error estimation. Overall, on top of being able
501 to identify new factors, the addition of the new specific proxies in the PMF strengthened the confidence we have for all other
502 factors.

503 3.4 Fine scale variability of the temporal contribution

504 Figure 3 indicates correlations of the concentrations for many chemical species across the sites. Additionally, the temporal
 505 evolution of the contribution of commonly resolved factors are further investigated in this section. Figure 8 presents the Pearson
 506 correlation coefficient of the contributions of the sources for the three pairs of sites. The sources that resulted to consistent
 507 strong correlations ($r > 0.77$) across all sites are biomass burning, nitrate-rich, aged sea salt, MSA-rich, secondary biogenic
 508 oxidation, and primary biogenic sources. The sea/road salt factor showed good correlations across the sites with a correlation
 509 coefficient ranging from 0.58 to 0.76.

510



511

512 **Figure 8: Heat map of the time series Pearson correlation coefficient of all factor contributions between LF and CB (LF-CB), LF**
 513 **and Vif (LF-Vif), and CB and Vif (CB-Vif).**

514

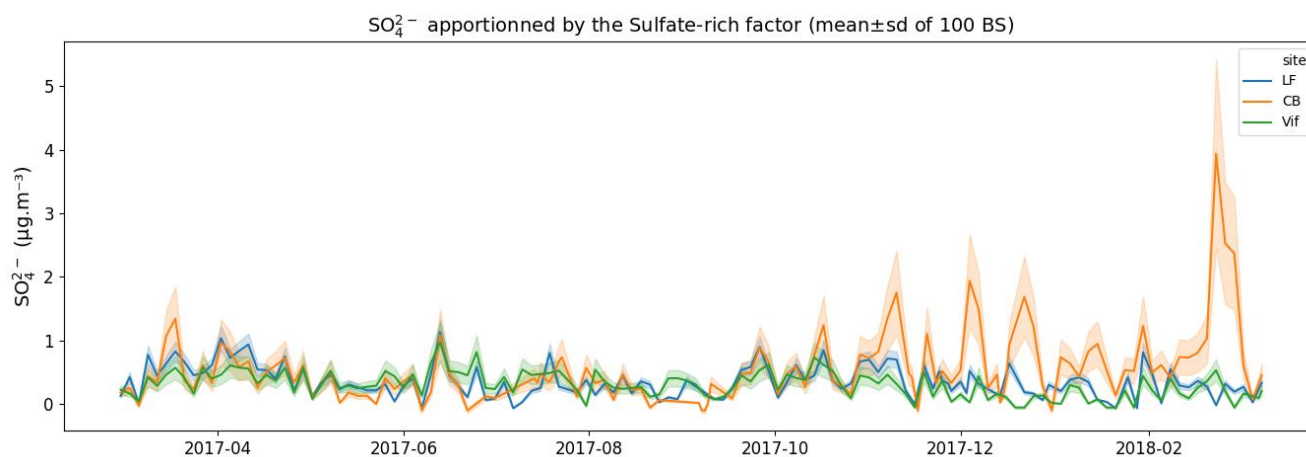
515 Factors with strong seasonality appeared to be highly correlated between sites (biomass burning, nitrate-rich, MSA-rich, and
 516 primary biogenic). This tends to affirm that such factors are dominated either by large scale transport (i.e., nitrate-rich) or by
 517 a strong climatic determinant. It is interesting to note that the primary biogenic factor presents systematically a slightly lower
 518 correlation than the polyols (LF-CB: $r_{polyols}=0.94$ to $r_{primary\ biogenic}=0.91$, LF-Vif: $r_{polyols}=0.92$ to $r_{primary\ biogenic}=0.88$ and Vif-CB:
 519 $r_{polyols}=0.87$ to $r_{primary\ biogenic}=0.82$). This may suggest a secondary process or a combination of several different primary
 520 processes in the primary biogenic factor affecting the sites at different rates (Petit et al., 2019; Samaké et al., 2019b). We also
 521 clearly see a stronger similarity between the two urban sites (LF and CB) compared to the peri urban one, notably for the
 522 primary traffic, mineral dust, and, to a lower extent, the industrial factor. This may be explained not only by the proximity of
 523 the location of the two former sites within the city, but also by their similarity in typology compared to the peri-urban site type
 524 in Vif. However, there are two factors that do not present good correlation between all sites.

525 One of them is the sulfate-rich factor which presents a similar contribution when comparing LF and Vif, but low-to-none
 526 correlation when compared to CB. A deeper analysis shows that the sulfate-rich, together with the nitrate-rich factor in CB,
 527 explains a large part of the winter spike of secondary inorganics (23/02/2018 to 24/02/2018), whereas in LF and Vif only the
 528 nitrate-rich factor explains most of it. This spike drives the Pearson correlation coefficient to a low value and without it, the

529 correlation increases drastically (see Figure S5.1 in the SI for the full scatterplot). Some PMF solutions of the BS in LF and
530 Vif also had this behaviour, but weren't chosen as the "best" solution. We propose two hypotheses for this difference: 1) during
531 winter, some heterogeneous chemistry may take place in fog episodes in the Grenoble basin (resulting to episodic spikes in
532 the SO_4^{2-} contribution), that may not be spatially homogeneous at a city scale, leading to mixing of secondary sources, and 2)
533 we have reached the limit of the PMF methodology to de-convolute further the secondary inorganics. Both hypotheses may be
534 concurrent.

535 A further indication of a potential mixing between the sulfate- and nitrate-rich factors is presented in Figure S5.3. In this figure,
536 the total mass concentration of PM and major ions (SO_4^{2-} , NO_3^- , and NH_4^+) were compared between sites when the sulfate-
537 and nitrate-rich factors were combined. Strong correlations between sites were found indicating similarity of such
538 concentrations in secondary sources. It is out of scope of this work to determine if this is a limitation of the PMF approach or
539 if there are some processes leading to real differences. We note however that apart from these spikes, the SO_4^{2-} apportioned
540 by this factor at 3 sites are in good agreement, and are within the uncertainties of each other (see Figure 9). This figure also
541 highlights that the uncertainty for the SO_4^{2-} in this factor is higher for the CB site, as also shown in the chemical profile in
542 Figure S3.6 in the SI.

543



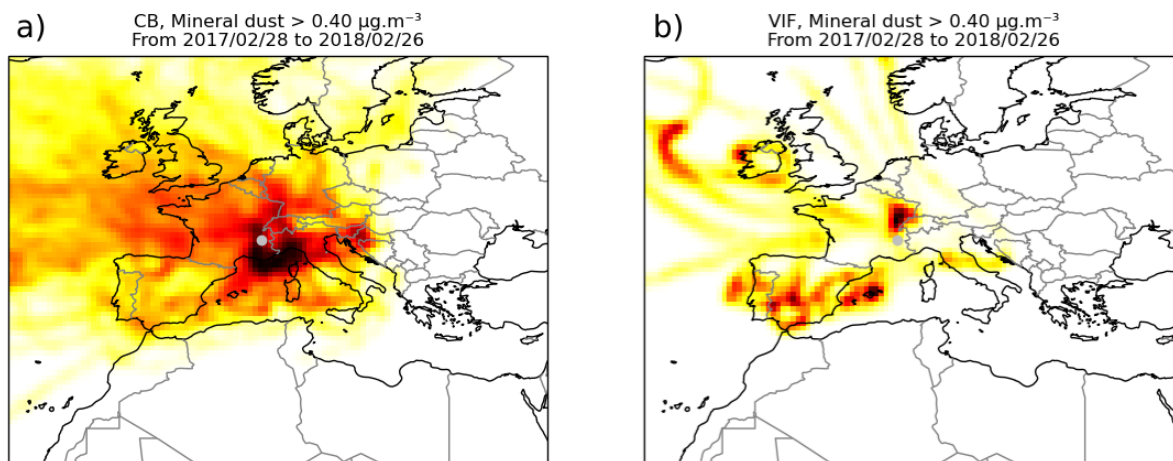
544

545 **Figure 9: SO_4^{2-} apportioned by the sulfate-rich factor at the 3 sites, according to the uncertainties given by the 100 BS as shown by**
546 **the mean (solid line) and the standard deviation (shaded area).**

547

548 The second factor which showed low correlations between pairs of sites is mineral dust, specifically when comparing Vif to
549 the two other sites. This is in line with the difference in the PM_{10} apportioned by this factor as shown in the previous section.
550 However, a closer look on the contribution scatterplot of $\text{Vif}_{\text{Mineral dust}}$ vs $\text{CB}_{\text{Mineral dust}}$ (see Figure S5.2 in the SI) highlights that
551 some events are very close to the 1:1 line. This is indicative of two regimes for mineral dust, with differences due to some
552 specificity in the atmospheric dynamics in the valley near the surface. To investigate it further, a potential source contribution

553 function (PSCF) analysis of the mineral dust factor for the Vif and CB sites was performed in order to assess the origin of air
554 masses of this factor (Figure 10). For the Vif site, the main origin is Spain with well-defined air flow canalized by the valley
555 and katabatic flows in a south to north direction (a phenomenon also reported in Largeron and Staquet (2016)). On the other
556 hand, the origin for CB is not as well-defined. These PSCF pattern tends to indicate that the sources of the mineral dust factor
557 present a strong local component for the urban sites (CB and LF being very similar), while the origin of the mineral dust factor
558 in Vif appears to be mainly affected by long-range transport of dust only.
559



560
561 **Figure 10: The PSCF analysis of the days with a mineral dust loading higher than 0.4 µg m⁻³ for the CB site (a) and Vif (b). Darker**
562 **shades indicate higher probability density of source origin.**

563
564 **3.5 Fine-scale variability of chemical profiles**

565 An additional similarity test was also performed to investigate the fine-scale variabilities of the chemical profiles of the factors.
566 A similarity analysis at a regional scale in France identified stable chemical profiles obtained by PMF studies across many
567 sites, corresponding to biomass burning, sulfate-rich, nitrate-rich, and fresh sea salt factors (Weber et al., 2019). In our study,
568 a parallel analysis was performed in order to evaluate the stability of the chemical profiles of the identified factors in high
569 proximity receptor locations. Briefly, PMF-resolved sources were compared for each pair of sites using both Pearson distance
570 (PD) and standardized identity distance (SID) to obtain a similarity metric (PD-SID).

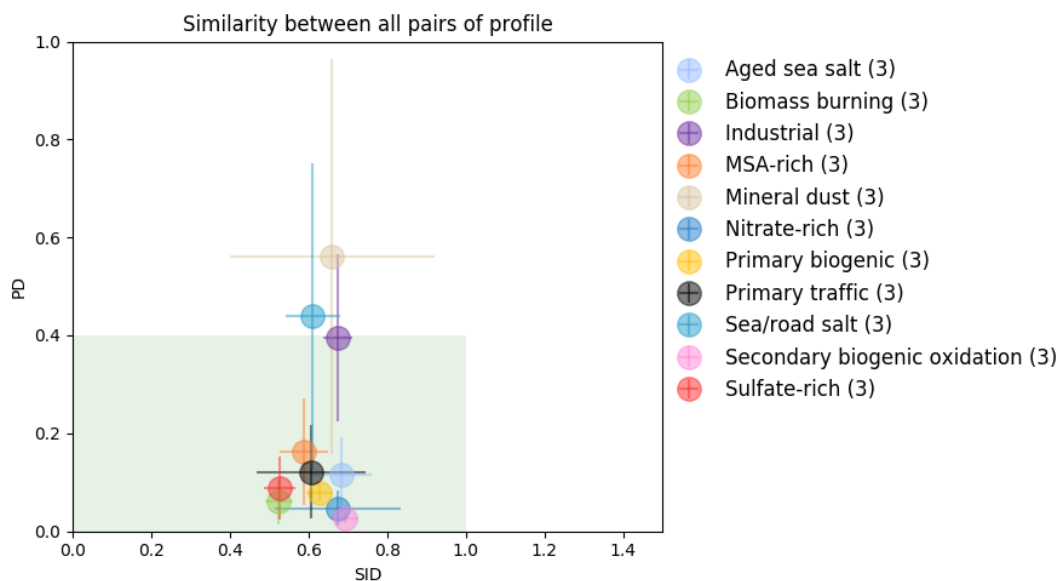
571 **3.5.1 (Dis-)similarity of the chemical profiles at the three sites**

572 Figure 11 presents the similarity plot (PD-SID) obtained for the 11 factors found in this study. The biomass burning factor
573 yielded the most stable chemical profile in all the sites in the Grenoble basin, which is consistent. Other stable factors include

574 sulfate- and nitrate-rich, primary biogenic, MSA-rich, and secondary biogenic oxidation. The industrial and sea/road salt
575 factors, both marginally above the accepted PD metric, could be considered as having heterogeneous profiles based on the
576 contributions of these sources to the total PM₁₀ in each site.

577 However, a clear heterogeneous chemical profile was found in the mineral dust, this further emphasized the difference in origin
578 of this factor as previously discussed in section 3.4. More details about of the chemical profile of this factor can be found
579 Figure S3.11 in the SI. One of the main differences is the lack of OC* in the Vif site compared to LF and CB sites, together
580 with a much lower Ca²⁺ contribution. Additionally, there is a lower SO₄²⁻ apportioned in the mineral dust factor in Vif. The
581 only similarity between all the sites are the high loadings of Al, Ti and V, as well as important contributions from other crustal
582 metals (Fe, Ni, Mn). It also has to be noted that the cellulose is present up to about 20% of its total mass in the mineral dust
583 profile in the CB site, however the BS estimates indicate very important uncertainties for this specie in this factor (see Figure
584 S3.11 in the SI).

585



586

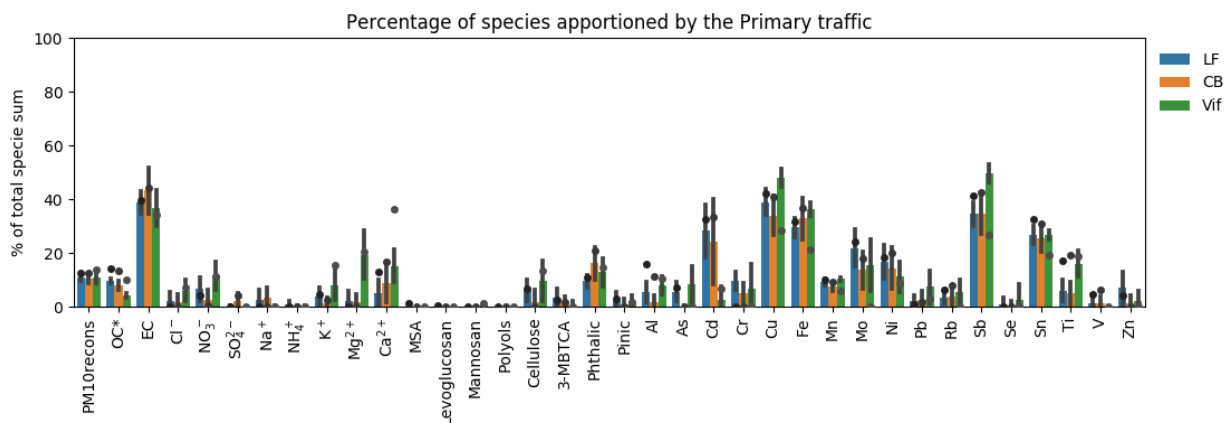
587 **Figure 11: Similarity plot of all chemical profiles in each site. The shaded area (in green) shows the acceptable range of the PD-SID**
588 **metric. For each point, the error bars represent the standard deviation of the 3 pairs of comparisons.**

589

590 Surprisingly, the sulfate-rich factor chemistry is one of the most stable profile, although its temporal contributions exhibits
591 high spatial variation, notably at CB compared to LF and Vif sites.

592 Finally, although the primary traffic factor showed a stable profile based on the similarity plot (PD-SID metric), it has to be
593 noted that, in the reference run (i.e., constrained), the specie concentrations are within the BS uncertainties for all species at
594 LF and CB sites, but outside the BS range for the Vif site (see Figure 12). Notably, the BS predicted higher contribution from

595 Cu, Fe, Sb and Sn, which are common tracers of tyre and brake wear, than the reference run. Additionally, the Ca^{2+} is
 596 overestimated in the reference run by a large amount, as well as the OC^* , and, to a lesser extent, the reconstructed PM_{10} . Such
 597 BS results indicate that, in Vif, the primary traffic factor is heavily influenced by this phenomenon on specific days, that has
 598 led to an overestimation of the total PM_{10} apportioned by this factor. Additionally, even at low concentrations, some terrestrial
 599 elements (Al, As, Ti) and cellulose are present in the primary traffic factor. As a result, even if the primary traffic characteristic
 600 of this factor is dominant, the influence of road dust re-suspension is not negligible for this factor in Vif.
 601



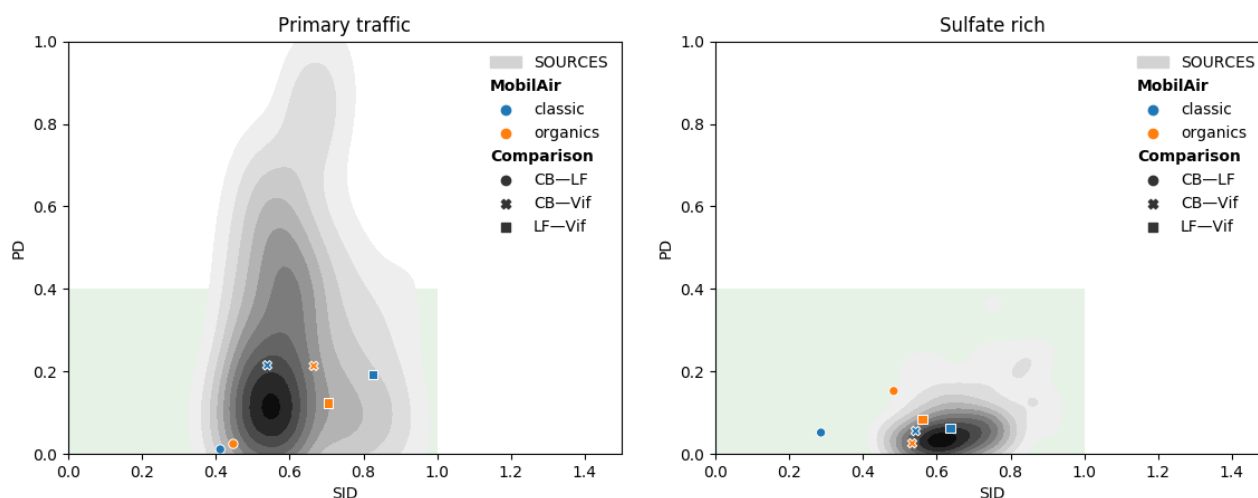
602
 603 **Figure 12: Percentage (%) of each specie apportioned by the primary traffic factor (dots refer to the constrained run, bar plots refer to the mean and error bars refer to the standard deviation of the 100 BS).**
 604

605
 606 **3.5.2. Comparison with other chemical profiles of PM_{10} sources from a regional study**

607 It is interesting to evaluate if a PMF study conducted at a city scale is leading to more similar source chemical profiles than a
 608 study using a database from a much larger area. Another question is whether PMF can produce more similar chemical source
 609 profiles with the help of additional organic tracers than a “classic” PMF run. Hence, the results obtained here are compared to
 610 those in the SOURCES program (Weber et al., 2019) for the 9 factors common in both studies (the secondary biogenic factor
 611 was not identified in the SOURCES program with the data sets not including its proper chemical tracers). This can be
 612 represented with the projection on a similarity plot of the distances between the factors for the 3 pairs of sites over the Grenoble
 613 basin, both for the “classic” and “orga” PMF. This is compared to the results from all possible pairs of sites within the 15 sites
 614 of the SOURCES study (distributed over France), mapped with a probability density function of similarities. Figure 13 presents
 615 these plots for the factors “primary traffic” and “sulfate-rich”, the other factors being presented in the SI (S6).

616 In most instances, the PMF results obtained for the Grenoble basin deliver slightly closer chemical profiles, both for the PD
 617 distance (sensitive to major components) and the SID distance (sensitive to the global profile), than the studies across more
 618 distant sites. This is particularly the case when comparing the two urban sites (LF and CB) (cf., Figure 11). Some values out
 619 of the acceptable range remain for some factors (mineral dust, industrial), involving the differences between the urban and

620 suburban sites, but are still fitting with the pattern obtained for the overall French sites. The addition of the organic tracers did
621 not alter the source profiles of the commonly resolved PMF factors and, in fact, even enhanced it by further refining the other
622 identified sources. This is predominantly seen in the MSA-rich factor, where some of the “classic” PMF results fell outside
623 the acceptable range while the “orga” PMF are all in the acceptable range of the similarity plot. The “orga” PMF run for some
624 factors such as primary biogenic, dust, and industrial factor also mostly yielded better PD and SID metrics (closer to the
625 acceptable range) than the “classic” PMF run.
626



627
628 **Figure 13: Similarity plots for the factor “Primary traffic” and “Sulfate-rich” for the pairs of sites formed in this study (Mobil’Air),**
629 **compared to the probability density function of similarities obtained for the 15 French sites of the SOURCES program.**

630 631 **3.6 Improvement of the identified sources with the new organic tracers**

632 In order to comprehensively apportion PM_{10} sources, the very large unknown portion of OM, especially in the secondary
633 fraction, needs to be properly identified. Most source apportionment studies only use standard input variables including OC,
634 EC, ions, and metals. However, these species alone are insufficient to describe the complexity of the organic matter, making
635 it a challenge to apportion sources from the OM fraction and their formation processes (i.e. primary or secondary origin)
636 (Srivastava et al., 2018a). Only a small number of studies have used organic tracers to apportion SOA in PM using PMF, and
637 even these studies usually have limited number of samples, number of tracers, and/or identified sources (Feng et al., 2013;
638 Shrivastava et al., 2007; Srivastava et al., 2018b). A few of these studies have proposed to estimate SOC contributions from
639 the sum of OC loadings in the secondary inorganic (nitrate- and sulfate-rich) factor (Hu et al., 2010; Ke et al., 2008; Lee et al.,
640 2008; Pachon et al., 2010; Yuan et al., 2006) or from water-soluble OC and humic-like substances (Qiao et al., 2018). Some
641 have estimated the contributions of biogenic SOA from the oxidation products of isoprene, alpha-pinene, and beta-

642 caryophyllene (Heo et al., 2013; Kleindienst et al., 2007; Miyazaki et al., 2012; Shrivastava et al., 2007; Wang et al., 2012).
643 In fact, the high contributions of biogenic SOA during warmer periods, that could range from 20-60% (Heo et al., 2013;
644 Miyazaki et al., 2012; Wang et al., 2012; Zhang et al., 2010), found by other PMF studies is also consistent with our findings.
645 Wang et al. (2017b) also highlighted the importance of biogenic SOA tracers as it significantly impacts the source
646 apportionment results, particularly in areas with strong SOA contributions. Although applied on a small sample size, an
647 interesting technique assimilating polar SOA tracers and primary organic aerosol (POA) tracers was performed by Hu et al.
648 (2010). This resulted to two identified SOA factors that are mixed with: 1) secondary inorganics and biomass burning, 2) green
649 waste and biomass burning. Hence, with the appropriate uncertainties, the SOA tracers can be a practical way, possibly even
650 necessary, to estimate SOA contributions (Feng et al., 2013) especially in urban areas (Wang et al., 2012).
651 Our study demonstrated that the use of organic tracers aided an effective source-specific approach that clearly identified major
652 sources of SOA in PM₁₀ such as MSA-rich and secondary biogenic oxidation sources. The potential influence of anthropogenic
653 emissions on some sources was also observed through the contribution of one of the organic tracers used, phthalic acid. The
654 sufficient number of samples (n>125 for each site) in our study have also maintained the statistical robustness of the solutions
655 obtained from filter-based measurements. The stability of the organic tracers also resulted to homogeneous chemical profiles
656 which allowed seamless identification of uncommonly resolved sources such as primary biogenic, secondary biogenic
657 oxidation, and MSA-rich. Although the addition of cellulose did not emerge as a separate biogenic factor, it provided an option
658 to scrutinize the difference in terms origin of the primary biogenic sources across sites. Overall, the organic tracers have further
659 refined the contribution of other identified sources by taking in consideration the SOA portion of PM₁₀ that would have
660 otherwise mixed with other sources and have facilitated an innovative approach to improve the apportionment of PM₁₀ sources.

661

662 **4 Conclusions**

663 A fine-scale source apportionment of PM₁₀ in different urban typologies (background, pedestrianized hyper-center, and peri-
664 urban) in a small scale area (<15 km) was performed using PMF 5.0. Additional organic tracers (MSA, cellulose, 3-MBTCA,
665 pinic acid, and phthalic acid) were used to supplement the standard input variables. An 11-factor optimal solution was found
666 for each of the three urban sites, including primary traffic, nitrate-rich, sulfate-rich, industrial, biomass burning, aged sea salt,
667 sea/road salt, mineral dust, primary biogenic, secondary biogenic oxidation, and MSA-rich sources. The results from
668 previously reported PMF studies in Grenoble (Shrivastava et al., 2018b; Weber et al., 2019) were confirmed by the findings in
669 this study particularly the long-term stability of regional source emissions 5 years apart. The PMF solution obtained with the
670 additional organic tracers resulted to:

- 671 1. the improvement of PM₁₀ mass closure and the exploration of appropriate input variable uncertainties;
- 672 2. the re-assignment of the bulk sulfate-rich factor contribution to more descriptive secondary aerosol sources in the
673 atmosphere;

- 674 3. the clear identification of commonly unresolved sources in the SOA fraction (e.g., primary biogenic, traced by the
675 polyols and cellulose; secondary biogenic oxidation, traced by 3-MBTCA and pinic acid; and MSA-rich, traced by
676 the MSA) in different urban typologies;
- 677 4. the decreased uncertainties, for both BS and DISP error estimates, that further strengthened confidence in the PMF
678 solution;
- 679 5. the increased knowledge of the stability of the chemical profiles of the factors, that could be a key when using them
680 in further large-scale analysis or modeling;

681 The 3 sites comparison at a local scale:

- 682 6. highlights very similar profiles and temporal evolution in the factor contributions at a conurbation scale (such as the
683 Grenoble basin);
- 684 7. allows the determination of local heterogeneities in a small scale area;
- 685 8. pointed out some difficulties to disentangle the secondary inorganic sources (NO_3^- and SO_4^{2-}) and some mixing
686 between both species may occur.

687 Overall, an enhanced and fine-scale source profile of PM_{10} was obtained in the Grenoble basin. The trend observed in the
688 MSA-rich, secondary biogenic oxidation, and primary biogenic factors showed the extent of this phenomenon suggesting
689 importance of the contribution of biogenic sources, both primary and secondary. The significant percentage attributed to SOA
690 sources revealed the strong necessity of organic molecular tracers in fully discriminating the origins of PM_{10} sources.

691 **Acknowledgements**

692 This work is supported by the French National Research Agency in the framework of the "Investissements d'avenir" program
693 (ANR-15-IDEX-02), for the Mobil'Air program. It also received support from the program QAMECS funded by ADEME
694 (convention 1662C0029), and from LCSQA and French Ministry of Environment for part of the analyses for the Les Frènes
695 site within the CARA program. Chemical analysis on the Air-O-Sol facility at IGE was made possible with the funding of
696 some of the equipment by the Labex OSUG@2020 (ANR10 LABX56). The PhD of SW is funded by ENS Paris. The internship
697 of T Cañete is taking place within the Erasmus exchange program. Finally, the authors would like to kindly thank the dedicated
698 efforts of many people from Atmo-AuRA at the sampling sites, and in the lab at IGE (A Vella, C Vérin, C Voiron) for collecting
699 and analysing the samples, respectively.

701 **Authors contributions**

702 GU, and JLJ designed the atmospheric chemistry part of the Mobil'Air program. SM and CT supervised the sampling at the 3
703 sites for Atmo AuRA. OF is the head of the CARA program that allows the collection of samples from Les Frènes site. VJ set
704 up the analytical techniques for polyols, sugars, and cellulose. TC performed the cellulose analyses. LJSB and SW processed

705 the data. SW developed some of the tools and ideas for in-depth PMF analysis. LJSB, SW, wrote the paper. JLJ and GU revised
706 the original draft. All authors reviewed and edited the manuscript.

707 **References**

708 Alleman, L. Y., Lamaison, L., Perdrix, E., Robache, A. and Galloo, J.-C.: PM10 metal concentrations and source identification
709 using positive matrix factorization and wind sectoring in a French industrial zone, *Atmospheric Research*, 96(4), 612–625,
710 <https://doi.org/10.1016/j.atmosres.2010.02.008>, 2010.

711 Atkinson, R. and Arey, J.: Atmospheric Chemistry of Biogenic Organic Compounds, *Acc. Chem. Res.*, 31(9), 574–583,
712 <https://doi.org/10.1021/ar970143z>, 1998.

713 Aymoz, G., Jaffrezo, J. L., Chapuis, D., Cozic, J. and Maenhaut, W.: Seasonal variation of PM₁₀ main constituents in two
714 valleys of the French Alps. I: EC/OC fractions, *Atmos. Chem. Phys.*, 7(3), 661–675, <https://doi.org/10.5194/acp-7-661-2007>,
715 2007.

716 Ayres, J. G., Borm, P., Cassee, F. R., Castranova, V., Donaldson, K., Ghio, A., Harrison, R. M., Hider, R., Kelly, F., Kooter,
717 I. M., Marano, F., Maynard, R. L., Mudway, I., Nel, A., Sioutas, C., Smith, S., Baeza-Squiban, A., Cho, A., Duggan, S. and
718 Froines, J.: Evaluating the Toxicity of Airborne Particulate Matter and Nanoparticles by Measuring Oxidative Stress
719 Potential—A Workshop Report and Consensus Statement, *Inhalation Toxicology*, 20(1), 75–99,
720 <https://doi.org/10.1080/08958370701665517>, 2008.

721 Barker, J. R., Steiner, A. L. and Wallington, T. J.: *Advances in Atmospheric Chemistry: Volume 2: Organic Oxidation and*
722 *Multiphase Chemistry*, WORLD SCIENTIFIC., 2019.

723 Belis, C. A., Favez, O., Harrison, R. M., Larsen, B. R., Amato, F., El Haddad, I., Hopke, P. K., Nava, S., Paatero, P., Prévôt,
724 A., Quass, U., Vecchi, R., Viana, M., European Commission, Joint Research Centre and Institute for Environment and
725 Sustainability: *European guide on air pollution source apportionment with receptor models.*, Publications Office,
726 Luxembourg, 2014.

727 Belis, C. A., Pernigotti, D., Karagulian, F., Pirovano, G., Larsen, B. R., Gerboles, M. and Hopke, P. K.: A new methodology
728 to assess the performance and uncertainty of source apportionment models in intercomparison exercises, *Atmospheric*
729 *Environment*, 119, 35–44, <https://doi.org/10.1016/j.atmosenv.2015.08.002>, 2015.

730 Belis, C. A., Pikridas, M., Lucarelli, F., Petralia, E., Cavalli, F., Calzolari, G., Berico, M. and Sciare, J.: Source apportionment
731 of fine PM by combining high time resolution organic and inorganic chemical composition datasets, *Atmospheric*
732 *Environment: X*, 3, 100046, <https://doi.org/10.1016/j.aeaoa.2019.100046>, 2019.

733 Belis, C. A., Pernigotti, D., Pirovano, G., Favez, O., Jaffrezo, J. L., Kuenen, J., Denier van Der Gon, H., Reizer, M., Riffault,
734 V., Alleman, L. Y., Almeida, M., Amato, F., Angyal, A., Argyropoulos, G., Bande, S., Beslic, I., Besombes, J.-L., Bove, M.
735 C., Brotto, P., Calori, G., Cesari, D., Colombi, C., Contini, D., De Gennaro, G., Di Gilio, A., Diapouli, E., El Haddad, I.,
736 Elbern, H., Eleftheriadis, K., Ferreira, J., Vivanco, M. G., Gilardoni, S., Golly, B., Hellebust, S., Hopke, P. K., Izadmanesh,
737 Y., Jorquera, H., Krajsek, K., Kranenburg, R., Lazzeri, P., Lenartz, F., Lucarelli, F., Maciejewska, K., Manders, A.,
738 Manousakas, M., Masiol, M., Mircea, M., Mooibroek, D., Nava, S., Oliveira, D., Paglione, M., Pandolfi, M., Perrone, M.,
739 Petralia, E., Pietrodangelo, A., Pillon, S., Pokorna, P., Prati, P., Salameh, D., Samara, C., Samek, L., Saraga, D., Sauvage, S.,
740 Schaap, M., Scotto, F., Sega, K., Siour, G., Tauler, R., Valli, G., Vecchi, R., Venturini, E., Vestenius, M., Waked, A. and
741 Yubero, E.: Evaluation of receptor and chemical transport models for PM10 source apportionment, *Atmospheric Environment:*
742 *X*, 5, 100053, <https://doi.org/10.1016/j.aeaoa.2019.100053>, 2020.

- 743 Bessagnet, B., Menut, L., Lapere, R., Couvidat, F., Jaffrezo, J.-L., Mailler, S., Favez, O., Pennel, R. and Siour, G.: High
744 Resolution Chemistry Transport Modeling with the On-Line CHIMERE-WRF Model over the French Alps—Analysis of a
745 Feedback of Surface Particulate Matter Concentrations on Mountain Meteorology, *Atmosphere*, 11(6), 565,
746 <https://doi.org/10.3390/atmos11060565>, 2020.
- 747 Birch, M. E. and Cary, R. A.: Elemental Carbon-Based Method for Monitoring Occupational Exposures to Particulate Diesel
748 Exhaust, *Aerosol Science and Technology*, 25(3), 221–241, <https://doi.org/10.1080/02786829608965393>, 1996.
- 749 Borlaza, L. J. S., Weber, S., Jaffrezo, J.-L., Houdier, S., Slama, R., Rieux, C., Albinet, A., Micallef, S., Trebuchon, C. and
750 Uzu, G.: Disparities in particulate matter (PM₁₀) origins and oxidative potential at a city-scale (Grenoble, France) - Part II:
751 Sources of PM₁₀ oxidative potential using multiple linear regression analysis and the predictive applicability of multilayer
752 perceptron neural network analysis, *Atmospheric Chemistry and Physics Discussions*, 2021.
- 753 Bove, M. C., Brotto, P., Cassola, F., Cuccia, E., Massabò, D., Mazzino, A., Piazzalunga, A. and Prati, P.: An integrated PM_{2.5}
754 source apportionment study: Positive Matrix Factorisation vs. the chemical transport model CAMx, *Atmospheric*
755 *Environment*, 94, 274–286, <https://doi.org/10.1016/j.atmosenv.2014.05.039>, 2014.
- 756 Bozzetti, C., Daellenbach, K. R., Hueglin, C., Fermo, P., Sciare, J., Kasper-Giebl, A., Mazar, Y., Abbaszade, G., El Kazzi, M.,
757 Gonzalez, R., Shuster-Meiseles, T., Flasch, M., Wolf, R., Křepelová, A., Canonaco, F., Schnelle-Kreis, J., Slowik, J. G.,
758 Zimmermann, R., Rudich, Y., Baltensperger, U., El Haddad, I. and Prévôt, A. S. H.: Size-Resolved Identification,
759 Characterization, and Quantification of Primary Biological Organic Aerosol at a European Rural Site, *Environ. Sci. Technol.*,
760 50(7), 3425–3434, <https://doi.org/10.1021/acs.est.5b05960>, 2016.
- 761 Bozzetti, C., Sosedova, Y., Xiao, M., Daellenbach, K. R., Ulevicius, V., Dudoitis, V., Mordas, G., Byčenkienė, S., Plauškaitė,
762 K., Vlachou, A., Golly, B., Chazeau, B., Besombes, J.-L., Baltensperger, U., Jaffrezo, J.-L., Slowik, J. G., El Haddad, I. and
763 Prévôt, A. S. H.: Argon offline-AMS source apportionment of organic aerosol over yearly cycles for an urban, rural, and
764 marine site in northern Europe, *Atmos. Chem. Phys.*, 17(1), 117–141, <https://doi.org/10.5194/acp-17-117-2017>, 2017.
- 765 Brunekreef, B.: Epidemiological evidence of effects of coarse airborne particles on health, *European Respiratory Journal*,
766 26(2), 309–318, <https://doi.org/10.1183/09031936.05.00001805>, 2005.
- 767 Budisulistiorini, S. H., Canagaratna, M. R., Croteau, P. L., Marth, W. J., Baumann, K., Edgerton, E. S., Shaw, S. L., Knipping,
768 E. M., Worsnop, D. R., Jayne, J. T., Gold, A. and Surratt, J. D.: Real-Time Continuous Characterization of Secondary Organic
769 Aerosol Derived from Isoprene Epoxydiols in Downtown Atlanta, Georgia, Using the Aerodyne Aerosol Chemical Speciation
770 Monitor, *Environ. Sci. Technol.*, 47(11), 5686–5694, <https://doi.org/10.1021/es400023n>, 2013.
- 771 Budisulistiorini, S. H., Baumann, K., Edgerton, E. S., Bairai, S. T., Mueller, S., Shaw, S. L., Knipping, E. M., Gold, A. and
772 Surratt, J. D.: Seasonal characterization of submicron aerosol chemical composition and organic aerosol sources in the
773 southeastern United States: Atlanta, Georgia, and Look Rock, Tennessee, *Atmos. Chem. Phys.*, 16(8), 5171–5189,
774 <https://doi.org/10.5194/acp-16-5171-2016>, 2016.
- 775 Bullock, K. R., Duvall, R. M., Norris, G. A., McDow, S. R. and Hays, M. D.: Evaluation of the CMB and PMF models using
776 organic molecular markers in fine particulate matter collected during the Pittsburgh Air Quality Study, *Atmospheric*
777 *Environment*, 42(29), 6897–6904, <https://doi.org/10.1016/j.atmosenv.2008.05.011>, 2008.
- 778 Calas, A., Uzu, G., Besombes, J.-L., Martins, J. M. F., Redaelli, M., Weber, S., Charron, A., Albinet, A., Chevrier, F., Brulfert,
779 G., Mesbah, B., Favez, O. and Jaffrezo, J.-L.: Seasonal Variations and Chemical Predictors of Oxidative Potential (OP) of
780 Particulate Matter (PM), for Seven Urban French Sites, , 20, 2019.

- 781 Cavalli, F., Viana, M., Yttri, K. E., Genberg, J. and Putaud, J.-P.: Toward a standardised thermal-optical protocol for measuring
782 atmospheric organic and elemental carbon: the EUSAAR protocol, *Atmos. Meas. Tech.*, 3(1), 79–89,
783 <https://doi.org/10.5194/amt-3-79-2010>, 2010.
- 784 Charron, A., Polo-Rehn, L., Besombes, J.-L., Golly, B., Buisson, C., Chanut, H., Marchand, N., Guillaud, G. and Jaffrezo, J.-
785 L.: Identification and quantification of particulate tracers of exhaust and non-exhaust vehicle emissions, *Atmos. Chem. Phys.*,
786 19(7), 5187–5207, <https://doi.org/10.5194/acp-19-5187-2019>, 2019.
- 787 Chen, Q., Sherwen, T., Evans, M. and Alexander, B.: DMS oxidation and sulfur aerosol formation in the marine troposphere:
788 a focus on reactive halogen and multiphase chemistry, *Atmos. Chem. Phys.*, 18(18), 13617–13637,
789 <https://doi.org/10.5194/acp-18-13617-2018>, 2018.
- 790 Chevrier, F.: Chauffage au bois et qualité de l'air en Vallée de l'Arve : définition d'un système de surveillance et impact d'une
791 politique de rénovation du parc des appareils anciens., PhD Thesis, Université Grenoble Alpes, Grenoble <https://tel.archives-ouvertes.fr/tel-01527559>, last access: 28 June 2018, 2016.
- 793 Colette, A., Menut, L., Haeffelin, M. and Morille, Y.: Impact of the transport of aerosols from the free troposphere towards
794 the boundary layer on the air quality in the Paris area, *Atmospheric Environment*, 42(2), 390–402,
795 <https://doi.org/10.1016/j.atmosenv.2007.09.044>, 2008.
- 796 Daellenbach, K. R., Kourtchev, I., Vogel, A. L., Bruns, E. A., Jiang, J., Petäjä, T., Jaffrezo, J.-L., Aksoyoglu, S., Kalberer, M.,
797 Baltensperger, U., El Haddad, I. and Prévôt, A. S. H.: Impact of anthropogenic and biogenic sources on the seasonal variation
798 in the molecular composition of urban organic aerosols: a field and laboratory study using ultra-high-resolution mass
799 spectrometry, *Atmos. Chem. Phys.*, 19(9), 5973–5991, <https://doi.org/10.5194/acp-19-5973-2019>, 2019.
- 800 Dai, Q., Liu, B., Bi, X., Wu, J., Liang, D., Zhang, Y., Feng, Y. and Hopke, P. K.: Dispersion Normalized PMF Provides
801 Insights into the Significant Changes in Source Contributions to PM_{2.5} after the COVID-19 Outbreak, *Environ. Sci. Technol.*,
802 [acs.est.0c02776](https://doi.org/10.1021/acs.est.0c02776), <https://doi.org/10.1021/acs.est.0c02776>, 2020a.
- 803 Dai, Q., Hopke, P. K., Bi, X. and Feng, Y.: Improving apportionment of PM_{2.5} using multisite PMF by constraining G-values
804 with a priori information, *Science of The Total Environment*, 736, 139657, <https://doi.org/10.1016/j.scitotenv.2020.139657>,
805 2020b.
- 806 van Drooge, B. L. and Grimalt, J. O.: Particle size-resolved source apportionment of primary and secondary organic tracer
807 compounds at urban and rural locations in Spain, *Atmos. Chem. Phys.*, 15(13), 7735–7752, <https://doi.org/10.5194/acp-15-7735-2015>, 2015.
- 809 Emami, F. and Hopke, P. K.: Effect of adding variables on rotational ambiguity in positive matrix factorization solutions,
810 *Chemometrics and Intelligent Laboratory Systems*, 162, 198–202, <https://doi.org/10.1016/j.chemolab.2017.01.012>, 2017.
- 811 Favez, O., El Haddad, I., Piot, C., Boréave, A., Abidi, E., Marchand, N., Jaffrezo, J.-L., Besombes, J.-L., Personnaz, M.-B.,
812 Sciare, J., Wortham, H., George, C. and D'Anna, B.: Inter-comparison of source apportionment models for the estimation of
813 wood burning aerosols during wintertime in an Alpine city (Grenoble, France), *Atmos. Chem. Phys.*, 10(12), 5295–5314,
814 <https://doi.org/10.5194/acp-10-5295-2010>, 2010.
- 815 Favez, O., Weber, S., Petit, J.-E., Alleman, L. Y., Albinet, A., Riffault, V., Chazeau, B., Amodeo, T., Salameh, D., Zhang, Y.,
816 Srivastava, D., Samaké, A., Aujay-Plouzeau, R., Papin, A., Bonnaire, N., Boullanger, C., Chatain, M., Chevrier, F., Detournay,
817 A., Dominik-Sègue, M., Falhun, R., Garbin, C., Gherzi, V., Grignion, G., Levigoureux, G., Pontet, S., Rangognio, J., Zhang,
818 S., Besombes, J.-L., Conil, S., Uzu, G., Savarino, J., Marchand, N., Gros, V., Marchand, C., Jaffrezo, J.-L. and Leoz-

- 819 Garziandia, E.: Overview of the French Operational Network for In Situ Observation of PM Chemical Composition and
820 Sources in Urban Environments (CARA Program), *Atmosphere*, 12(2), 207, <https://doi.org/10.3390/atmos12020207>, 2021.
- 821 Feng, J., Li, M., Zhang, P., Gong, S., Zhong, M., Wu, M., Zheng, M., Chen, C., Wang, H. and Lou, S.: Investigation of the
822 sources and seasonal variations of secondary organic aerosols in PM_{2.5} in Shanghai with organic tracers, *Atmospheric*
823 *Environment*, 79, 614–622, <https://doi.org/10.1016/j.atmosenv.2013.07.022>, 2013.
- 824 Franchini, M. and Mannucci, P.: Particulate Air Pollution and Cardiovascular Risk: Short-term and Long-term Effects, *Semin*
825 *Thromb Hemost*, 35(07), 665–670, <https://doi.org/10.1055/s-0029-1242720>, 2009.
- 826 Gelencsér, A., May, B., Simpson, D., Sánchez-Ochoa, A., Kasper-Giebl, A., Puxbaum, H., Caseiro, A., Pio, C. and Legrand,
827 M.: Source apportionment of PM_{2.5} organic aerosol over Europe: Primary/secondary, natural/anthropogenic, and
828 fossil/biogenic origin, *J. Geophys. Res.*, 112(D23), D23S04, <https://doi.org/10.1029/2006JD008094>, 2007.
- 829 Gianini, M. F. D., Fischer, A., Gehrig, R., Ulrich, A., Wichser, A., Piot, C., Besombes, J.-L. and Hueglin, C.: Comparative
830 source apportionment of PM₁₀ in Switzerland for 2008/2009 and 1998/1999 by Positive Matrix Factorisation, *Atmospheric*
831 *Environment*, 54, 149–158, <https://doi.org/10.1016/j.atmosenv.2012.02.036>, 2012.
- 832 Golly, B., Waked, A., Weber, S., Samake, A., Jacob, V., Conil, S., Rangognio, J., Chrétien, E., Vagnot, M.-P., Robic, P.-Y.,
833 Besombes, J.-L. and Jaffrezo, J.-L.: Organic markers and OC source apportionment for seasonal variations of PM_{2.5} at 5 rural
834 sites in France, *Atmospheric Environment*, 198, 142–157, <https://doi.org/10.1016/j.atmosenv.2018.10.027>, 2019.
- 835 Graham, B., Guyon, P., Taylor, P. E., Artaxo, P., Maenhaut, W., Glovsky, M. M., Flagan, R. C. and Andreae, M. O.: Organic
836 compounds present in the natural Amazonian aerosol: Characterization by gas chromatography-mass spectrometry:
837 ORGANIC COMPOUNDS IN AMAZONIAN AEROSOLS, *J. Geophys. Res.*, 108(D24), n/a-n/a,
838 <https://doi.org/10.1029/2003JD003990>, 2003.
- 839 Grover, B. D.: Measurement of total PM_{2.5} mass (nonvolatile plus semivolatile) with the Filter Dynamic Measurement System
840 tapered element oscillating microbalance monitor, *J. Geophys. Res.*, 110(D7), D07S03,
841 <https://doi.org/10.1029/2004JD004995>, 2005.
- 842 Heo, J., Dulger, M., Olson, M. R., McGinnis, J. E., Shelton, B. R., Matsunaga, A., Sioutas, C. and Schauer, J. J.: Source
843 apportionments of PM_{2.5} organic carbon using molecular marker Positive Matrix Factorization and comparison of results from
844 different receptor models, *Atmospheric Environment*, 73, 51–61, <https://doi.org/10.1016/j.atmosenv.2013.03.004>, 2013.
- 845 Hopke, P. K.: Review of receptor modeling methods for source apportionment, *Journal of the Air & Waste Management*
846 *Association*, 66(3), 237–259, <https://doi.org/10.1080/10962247.2016.1140693>, 2016.
- 847 Horne, J. R. and Dabdub, D.: Impact of global climate change on ozone, particulate matter, and secondary organic aerosol
848 concentrations in California: A model perturbation analysis, *Atmospheric Environment*, 153, 1–17,
849 <https://doi.org/10.1016/j.atmosenv.2016.12.049>, 2017.
- 850 Hu, D., Bian, Q., Lau, A. K. H. and Yu, J. Z.: Source apportioning of primary and secondary organic carbon in summer PM
851 _{2.5} in Hong Kong using positive matrix factorization of secondary and primary organic tracer data, *J. Geophys. Res.*, 115(D16),
852 D16204, <https://doi.org/10.1029/2009JD012498>, 2010.
- 853 Hyder, M., Genberg, J., Sandahl, M., Swietlicki, E. and Jönsson, J. Å.: Yearly trend of dicarboxylic acids in organic aerosols
854 from south of Sweden and source attribution, *Atmospheric Environment*, 57, 197–204,
855 <https://doi.org/10.1016/j.atmosenv.2012.04.027>, 2012.

- 856 Ishizuka, T., Kabashima, H., Yamaguchi, T., Tanabe, K. and Hattori, H.: Initial Step of Flue Gas Desulfurization An IR Study
857 of the Reaction of SO₂ with NO_x on CaO, *Environ. Sci. Technol.*, 34(13), 2799–2803, <https://doi.org/10.1021/es991073p>,
858 2000.
- 859 Jaffrezo, J. L., Calas, N. and Bouchet, M.: Carboxylic acids measurements with ionic chromatography, *Atmospheric*
860 *Environment*, 32(14), 2705–2708, 1998.
- 861 Jardine, K., Yañez-Serrano, A. M., Williams, J., Kunert, N., Jardine, A., Taylor, T., Abrell, L., Artaxo, P., Guenther, A.,
862 Hewitt, C. N., House, E., Florentino, A. P., Manzi, A., Higuchi, N., Kesselmeier, J., Behrendt, T., Veres, P. R., Derstroff, B.,
863 Fuentes, J. D., Martin, S. T. and Andreae, M. O.: Dimethyl sulfide in the Amazon rain forest: DMS in the Amazon, *Global*
864 *Biogeochem. Cycles*, 29(1), 19–32, <https://doi.org/10.1002/2014GB004969>, 2015.
- 865 Jin, X., Xue, B., Zhou, Q., Su, R. and Li, Z.: Mitochondrial damage mediated by ROS incurs bronchial epithelial cell apoptosis
866 upon ambient PM_{2.5} exposure, *J. Toxicol. Sci.*, 43(2), 101–111, <https://doi.org/10.2131/jts.43.101>, 2018.
- 867 Ke, L., Liu, W., Wang, Y., Russell, A. G., Edgerton, E. S. and Zheng, M.: Comparison of PM_{2.5} source apportionment using
868 positive matrix factorization and molecular marker-based chemical mass balance, *Science of The Total Environment*, 394(2–
869 3), 290–302, <https://doi.org/10.1016/j.scitotenv.2008.01.030>, 2008.
- 870 Kleindienst, T. E., Jaoui, M., Lewandowski, M., Offenberg, J. H., Lewis, C. W., Bhave, P. V. and Edney, E. O.: Estimates of
871 the contributions of biogenic and anthropogenic hydrocarbons to secondary organic aerosol at a southeastern US location,
872 *Atmospheric Environment*, 41(37), 8288–8300, <https://doi.org/10.1016/j.atmosenv.2007.06.045>, 2007.
- 873 Kunit, M. and Puxbaum, H.: Enzymatic determination of the cellulose content of atmospheric aerosols, *Atmospheric*
874 *Environment*, 30(8), 1233–1236, [https://doi.org/10.1016/1352-2310\(95\)00429-7](https://doi.org/10.1016/1352-2310(95)00429-7), 1996.
- 875 Langrish, J. P., Bosson, J., Unosson, J., Muala, A., Newby, D. E., Mills, N. L., Blomberg, A. and Sandström, T.: Cardiovascular
876 effects of particulate air pollution exposure: time course and underlying mechanisms, *Journal of Internal Medicine*, 272(3),
877 224–239, <https://doi.org/10.1111/j.1365-2796.2012.02566.x>, 2012.
- 878 Llargeron, Y. and Staquet, C.: The Atmospheric Boundary Layer during Wintertime Persistent Inversions in the Grenoble
879 Valleys, *Front. Earth Sci.*, 4, <https://doi.org/10.3389/feart.2016.00070>, 2016.
- 880 Lee, S., Liu, W., Wang, Y., Russell, A. G. and Edgerton, E. S.: Source apportionment of PM_{2.5}: Comparing PMF and CMB
881 results for four ambient monitoring sites in the southeastern United States, *Atmospheric Environment*, 42(18), 4126–4137,
882 <https://doi.org/10.1016/j.atmosenv.2008.01.025>, 2008.
- 883 Li, S.-M., Barrie, L. A., Talbot, R. W., Harriss, R. C., Davidson, C. I. and Jaffrezo, J.-L.: Seasonal and geographic variations
884 of methanesulfonic acid in the arctic troposphere, *Atmospheric Environment. Part A. General Topics*, 27(17–18), 3011–3024,
885 [https://doi.org/10.1016/0960-1686\(93\)90333-T](https://doi.org/10.1016/0960-1686(93)90333-T), 1993.
- 886 Marmur, A., Mulholland, J. A. and Russell, A. G.: Optimized variable source-profile approach for source apportionment,
887 *Atmospheric Environment*, 41(3), 493–505, <https://doi.org/10.1016/j.atmosenv.2006.08.028>, 2007.
- 888 McNeill, V. F.: Atmospheric Aerosols: Clouds, Chemistry, and Climate, *Annu. Rev. Chem. Biomol. Eng.*, 8(1), 427–444,
889 <https://doi.org/10.1146/annurev-chembioeng-060816-101538>, 2017.
- 890 Miyazaki, Y., Fu, P. Q., Kawamura, K., Mizoguchi, Y. and Yamanoi, K.: Seasonal variations of stable carbon isotopic
891 composition and biogenic tracer compounds of water-soluble organic aerosols in a deciduous forest, *Atmos. Chem. Phys.*,
892 12(3), 1367–1376, <https://doi.org/10.5194/acp-12-1367-2012>, 2012.

- 893 Nel, A.: ATMOSPHERE: Enhanced: Air Pollution-Related Illness: Effects of Particles, *Science*, 308(5723), 804–806,
894 <https://doi.org/10.1126/science.1108752>, 2005.
- 895 Norris, G., Duvall, R., Brown, S. and Bai, S.: Positive Matrix Factorization (PMF) 5.0 Fundamentals and User Guide, , 136,
896 2014.
- 897 Ostro, B., Tobias, A., Querol, X., Alastuey, A., Amato, F., Pey, J., Pérez, N. and Sunyer, J.: The Effects of Particulate Matter
898 Sources on Daily Mortality: A Case-Crossover Study of Barcelona, Spain, *Environmental Health Perspectives*, 119(12), 1781–
899 1787, <https://doi.org/10.1289/ehp.1103618>, 2011.
- 900 Paatero, P.: The Multilinear Engine—A Table-Driven, Least Squares Program for Solving Multilinear Problems, Including
901 the n -Way Parallel Factor Analysis Model, *Journal of Computational and Graphical Statistics*, 8(4), 854–888,
902 <https://doi.org/10.1080/10618600.1999.10474853>, 1999.
- 903 Paatero, P. and Tapper, U.: Positive matrix factorization: A non-negative factor model with optimal utilization of error
904 estimates of data values, *Environmetrics*, 5(2), 111–126, <https://doi.org/10.1002/env.3170050203>, 1994.
- 905 Pachon, J. E., Balachandran, S., Hu, Y., Weber, R. J., Mulholland, J. A. and Russell, A. G.: Comparison of SOC estimates and
906 uncertainties from aerosol chemical composition and gas phase data in Atlanta, *Atmospheric Environment*, 44(32), 3907–
907 3914, <https://doi.org/10.1016/j.atmosenv.2010.07.017>, 2010.
- 908 Pandolfi, M., Mooibroek, D., Hopke, P., van Pinxteren, D., Querol, X., Herrmann, H., Alastuey, A., Favez, O., Hüglin, C.,
909 Perdrix, E., Riffault, V., Sauvage, S., van der Swaluw, E., Tarasova, O. and Colette, A.: Long-range and local air pollution:
910 what can we learn from chemical speciation of particulate matter at paired sites?, *Atmos. Chem. Phys.*, 20(1), 409–429,
911 <https://doi.org/10.5194/acp-20-409-2020>, 2020.
- 912 Pernigotti, D. and Belis, C. A.: DeltaSA tool for source apportionment benchmarking, description and sensitivity analysis,
913 *Atmospheric Environment*, 180, 138–148, <https://doi.org/10.1016/j.atmosenv.2018.02.046>, 2018.
- 914 Pernigotti, D., Belis, C. A. and Spanò, L.: SPECIEUROPE: The European data base for PM source profiles, *Atmospheric
915 Pollution Research*, 7(2), 307–314, <https://doi.org/10.1016/j.apr.2015.10.007>, 2016.
- 916 Petit, J.-E., Pallarès, C., Favez, O., Alleman, L. Y., Bonnaire, N. and Rivière, E.: Sources and Geographical Origins of PM10
917 in Metz (France) Using Oxalate as a Marker of Secondary Organic Aerosols by Positive Matrix Factorization Analysis,
918 *Atmosphere*, 10(7), 370, <https://doi.org/10.3390/atmos10070370>, 2019.
- 919 Pey, J., Alastuey, A. and Querol, X.: PM10 and PM2.5 sources at an insular location in the western Mediterranean by using
920 source apportionment techniques, *Science of The Total Environment*, 456–457, 267–277,
921 <https://doi.org/10.1016/j.scitotenv.2013.03.084>, 2013.
- 922 Piao, M. J., Ahn, M. J., Kang, K. A., Ryu, Y. S., Hyun, Y. J., Shilnikova, K., Zhen, A. X., Jeong, J. W., Choi, Y. H., Kang, H.
923 K., Koh, Y. S. and Hyun, J. W.: Particulate matter 2.5 damages skin cells by inducing oxidative stress, subcellular organelle
924 dysfunction, and apoptosis, *Arch Toxicol*, 92(6), 2077–2091, <https://doi.org/10.1007/s00204-018-2197-9>, 2018.
- 925 Pindado, O. and Perez, R. M.: Source apportionment of particulate organic compounds in a rural area of Spain by positive
926 matrix factorization, *Atmospheric Pollution Research*, 2(4), 492–505, <https://doi.org/10.5094/APR.2011.056>, 2011.
- 927 Putaud, J.-P., Van Dingenen, R., Alastuey, A., Bauer, H., Birmili, W., Cyrys, J., Flentje, H., Fuzzi, S., Gehrig, R., Hansson,
928 H. C., Harrison, R. M., Herrmann, H., Hitzenberger, R., Hüglin, C., Jones, A. M., Kasper-Giebl, A., Kiss, G., Koussa, A.,
929 Kuhlbusch, T. A. J., Löschau, G., Maenhaut, W., Molnar, A., Moreno, T., Pekkanen, J., Perrino, C., Pitz, M., Puxbaum, H.,

- 930 Querol, X., Rodriguez, S., Salma, I., Schwarz, J., Smolik, J., Schneider, J., Spindler, G., ten Brink, H., Tursic, J., Viana, M.,
931 Wiedensohler, A. and Raes, F.: A European aerosol phenomenology – 3: Physical and chemical characteristics of particulate
932 matter from 60 rural, urban, and kerbside sites across Europe, *Atmospheric Environment*, 44(10), 1308–1320,
933 <https://doi.org/10.1016/j.atmosenv.2009.12.011>, 2010.
- 934 Puxbaum, H.: Size distribution and seasonal variation of atmospheric cellulose, *Atmospheric Environment*, 37(26), 3693–
935 3699, [https://doi.org/10.1016/S1352-2310\(03\)00451-5](https://doi.org/10.1016/S1352-2310(03)00451-5), 2003.
- 936 Qiao, F., Li, Q. and Lei, Y.: Particulate Matter Caused Health Risk in an Urban Area of the Middle East and the Challenges in
937 Reducing its Anthropogenic Emissions, *Environ Pollut Climate Change*, 02(01), <https://doi.org/10.4172/2573-458X.1000145>,
938 2018.
- 939 Saeaw, N. and Thepanondh, S.: Source apportionment analysis of airborne VOCs using positive matrix factorization in
940 industrial and urban areas in Thailand, *Atmospheric Pollution Research*, 6(4), 644–650,
941 <https://doi.org/10.5094/APR.2015.073>, 2015.
- 942 Samaké, A., Jaffrezo, J.-L., Favez, O., Weber, S., Jacob, V., Canete, T., Albinet, A., Charron, A., Riffault, V., Perdrix, E.,
943 Waked, A., Golly, B., Salameh, D., Chevrier, F., Oliveira, D. M., Besombes, J.-L., Martins, J. M. F., Bonnaire, N., Conil, S.,
944 Guillaud, G., Mesbah, B., Rocq, B., Robic, P.-Y., Hulin, A., Le Meur, S., Descheemaeker, M., Chretien, E., Marchand, N.
945 and Uzu, G.: Arabitol, mannitol, and glucose as tracers of primary biogenic organic aerosol: the influence of environmental
946 factors on ambient air concentrations and spatial distribution over France, *Atmos. Chem. Phys.*, 19(16), 11013–11030,
947 <https://doi.org/10.5194/acp-19-11013-2019>, 2019a.
- 948 Samaké, A., Jaffrezo, J.-L., Favez, O., Weber, S., Jacob, V., Albinet, A., Riffault, V., Perdrix, E., Waked, A., Golly, B.,
949 Salameh, D., Chevrier, F., Oliveira, D. M., Bonnaire, N., Besombes, J.-L., Martins, J. M. F., Conil, S., Guillaud, G., Mesbah,
950 B., Rocq, B., Robic, P.-Y., Hulin, A., Le Meur, S., Descheemaeker, M., Chretien, E., Marchand, N. and Uzu, G.: Polyols and
951 glucose particulate species as tracers of primary biogenic organic aerosols at 28 French sites, *Atmos. Chem. Phys.*, 19(5),
952 3357–3374, <https://doi.org/10.5194/acp-19-3357-2019>, 2019b.
- 953 Schauer, J. J. and Cass, G. R.: Source Apportionment of Wintertime Gas-Phase and Particle-Phase Air Pollutants Using
954 Organic Compounds as Tracers, *Environ. Sci. Technol.*, 34(9), 1821–1832, <https://doi.org/10.1021/es981312t>, 2000.
- 955 Schneider, W. F., Li, J. and Hass, K. C.: Combined Computational and Experimental Investigation of SO_x Adsorption on
956 MgO, *J. Phys. Chem. B*, 105(29), 6972–6979, <https://doi.org/10.1021/jp010747r>, 2001.
- 957 Seinfeld, J. H. and Pankow, J. F.: ORGANIC ATMOSPHERIC PARTICULATE MATERIAL, *Annu. Rev. Phys. Chem.*,
958 54(1), 121–140, <https://doi.org/10.1146/annurev.physchem.54.011002.103756>, 2003.
- 959 Shiraiwa, M., Ueda, K., Pozzer, A., Lammel, G., Kampf, C. J., Fushimi, A., Enami, S., Arangio, A. M., Fröhlich-Nowoisky,
960 J., Fujitani, Y., Furuyama, A., Lakey, P. S. J., Lelieveld, J., Lucas, K., Morino, Y., Pöschl, U., Takahama, S., Takami, A.,
961 Tong, H., Weber, B., Yoshino, A. and Sato, K.: Aerosol Health Effects from Molecular to Global Scales, *Environ. Sci.*
962 *Technol.*, 51(23), 13545–13567, <https://doi.org/10.1021/acs.est.7b04417>, 2017.
- 963 Shrivastava, M. K., Subramanian, R., Rogge, W. F. and Robinson, A. L.: Sources of organic aerosol: Positive matrix
964 factorization of molecular marker data and comparison of results from different source apportionment models, *Atmospheric*
965 *Environment*, 41(40), 9353–9369, <https://doi.org/10.1016/j.atmosenv.2007.09.016>, 2007.
- 966 Srivastava, D., Favez, O., Perraudin, E., Villenave, E. and Albinet, A.: Comparison of Measurement-Based Methodologies to
967 Apportion Secondary Organic Carbon (SOC) in PM_{2.5}: A Review of Recent Studies, *Atmosphere*, 9(11), 452,
968 <https://doi.org/10.3390/atmos9110452>, 2018a.

- 969 Srivastava, D., Tomaz, S., Favez, O., Lanzafame, G. M., Golly, B., Besombes, J.-L., Alleman, L. Y., Jaffrezo, J.-L., Jacob, V.,
970 Perraudin, E., Villenave, E. and Albinet, A.: Speciation of organic fraction does matter for source apportionment. Part 1: A
971 one-year campaign in Grenoble (France), *Science of The Total Environment*, 624, 1598–1611,
972 <https://doi.org/10.1016/j.scitotenv.2017.12.135>, 2018b.
- 973 Surratt, J. D., Chan, A. W. H., Eddingsaas, N. C., Chan, M., Loza, C. L., Kwan, A. J., Hersey, S. P., Flagan, R. C., Wennberg,
974 P. O. and Seinfeld, J. H.: Reactive intermediates revealed in secondary organic aerosol formation from isoprene, *Proceedings*
975 *of the National Academy of Sciences*, 107(15), 6640–6645, <https://doi.org/10.1073/pnas.0911114107>, 2010.
- 976 Szmigielski, R., Surratt, J. D., Gómez-González, Y., Van der Veken, P., Kourtchev, I., Vermeylen, R., Blockhuys, F., Jaoui,
977 M., Kleindienst, T. E., Lewandowski, M., Offenberg, J. H., Edney, E. O., Seinfeld, J. H., Maenhaut, W. and Claeys, M.: 3-
978 methyl-1,2,3-butanetricarboxylic acid: An atmospheric tracer for terpene secondary organic aerosol, *Geophys. Res. Lett.*,
979 34(24), L24811, <https://doi.org/10.1029/2007GL031338>, 2007.
- 980 Tomaz, S., Shahpoury, P., Jaffrezo, J.-L., Lammel, G., Perraudin, E., Villenave, E. and Albinet, A.: One-year study of
981 polycyclic aromatic compounds at an urban site in Grenoble (France): Seasonal variations, gas/particle partitioning and cancer
982 risk estimation, *Science of The Total Environment*, 565, 1071–1083, <https://doi.org/10.1016/j.scitotenv.2016.05.137>, 2016.
- 983 Tomaz, S., Jaffrezo, J.-L., Favez, O., Perraudin, E., Villenave, E. and Albinet, A.: Sources and atmospheric chemistry of oxy-
984 and nitro-PAHs in the ambient air of Grenoble (France), *Atmospheric Environment*, 161, 144–154,
985 <https://doi.org/10.1016/j.atmosenv.2017.04.042>, 2017.
- 986 Ullerstam, M., Vogt, R., Langer, S. and Ljungström, E.: The kinetics and mechanism of SO₂ oxidation by O₃ on mineral dust,
987 *Phys. Chem. Chem. Phys.*, 4(19), 4694–4699, <https://doi.org/10.1039/B203529B>, 2002.
- 988 Ullerstam, M., Johnson, M. S., Vogt, R. and Ljungström, E.: DRIFTS and Knudsen cell study of the heterogeneous reactivity
989 of SO₂ and NO₂ on mineral dust, *Atmos. Chem. Phys.*, 3(6), 2043–2051, <https://doi.org/10.5194/acp-3-2043-2003>, 2003.
- 990 Usher, C. R., Al-Hosney, H., Carlos-Cuellar, S. and Grassian, V. H.: A laboratory study of the heterogeneous uptake and
991 oxidation of sulfur dioxide on mineral dust particles: UPTAKE OF SULFUR DIOXIDE ON DUST, *J.-Geophys.-Res.*,
992 107(D23), ACH 16-1-ACH 16-9, <https://doi.org/10.1029/2002JD002051>, 2002.
- 993 Verma, S. K., Kawamura, K., Chen, J. and Fu, P.: Thirteen years of observations on primary sugars and sugar alcohols over
994 remote Chichijima Island in the western North Pacific, *Atmos. Chem. Phys.*, 18(1), 81–101, [https://doi.org/10.5194/acp-18-](https://doi.org/10.5194/acp-18-81-2018)
995 81-2018, 2018.
- 996 Vlachou, A., Tobler, A., Lamkaddam, H., Canonaco, F., Daellenbach, K. R., Jaffrezo, J.-L., Minguillón, M. C., Maasikmets,
997 M., Teinmaa, E., Baltensperger, U., El Haddad, I. and Prévôt, A. S. H.: Development of a versatile source apportionment
998 analysis based on positive matrix factorization: a case study of the seasonal variation of organic aerosol sources in Estonia,
999 *Atmos. Chem. Phys. Discuss.*, 1–21, <https://doi.org/10.5194/acp-2018-1099>, 2018.
- 1000 Waked, A., Favez, O., Alleman, L. Y., Piot, C., Petit, J.-E., Delaunay, T., Verlinden, E., Golly, B., Besombes, J.-L., Jaffrezo,
1001 J.-L. and Leoz-Garziandia, E.: Source apportionment of PM₁₀ in a north-western Europe regional
1002 urban background site (Lens, France) using positive matrix factorization and including primary biogenic emissions, *Atmos.*
1003 *Chem. Phys.*, 14(7), 3325–3346, <https://doi.org/10.5194/acp-14-3325-2014>, 2014.
- 1004 Wang, Q., Jiang, N., Yin, S., Li, X., Yu, F., Guo, Y. and Zhang, R.: Carbonaceous species in PM_{2.5} and PM₁₀ in urban area
1005 of Zhengzhou in China: Seasonal variations and source apportionment, *Atmospheric Research*, 191, 1–11,
1006 <https://doi.org/10.1016/j.atmosres.2017.02.003>, 2017a.

- 1007 Wang, Q., He, X., Huang, X. H. H., Griffith, S. M., Feng, Y., Zhang, T., Zhang, Q., Wu, D. and Yu, J. Z.: Impact of Secondary
1008 Organic Aerosol Tracers on Tracer-Based Source Apportionment of Organic Carbon and PM_{2.5}: A Case Study in the Pearl
1009 River Delta, China, *ACS Earth Space Chem.*, 1(9), 562–571, <https://doi.org/10.1021/acsearthspacechem.7b00088>, 2017b.
- 1010 Wang, Y., Hopke, P. K., Xia, X., Rattigan, O. V., Chalupa, D. C. and Utell, M. J.: Source apportionment of airborne particulate
1011 matter using inorganic and organic species as tracers, *Atmospheric Environment*, 55, 525–532,
1012 <https://doi.org/10.1016/j.atmosenv.2012.03.073>, 2012.
- 1013 Warneck, P.: *Chemistry of the natural atmosphere*, 2nd ed., Academic Press, San Diego., 2000.
- 1014 Weber, S., Salameh, D., Albinet, A., Alleman, L. Y., Waked, A., Besombes, J.-L., Jacob, V., Guillaud, G., Meshbah, B., Rocq,
1015 B., Hulin, A., Dominik-Sègue, M., Chrétien, E., Jaffrezo, J.-L. and Favez, O.: Comparison of PM₁₀ Sources Profiles at 15
1016 French Sites Using a Harmonized Constrained Positive Matrix Factorization Approach, *Atmosphere*, 10(6), 310,
1017 <https://doi.org/10.3390/atmos10060310>, 2019.
- 1018 Willers, S. M., Eriksson, C., Gidhagen, L., Nilsson, M. E., Pershagen, G. and Bellander, T.: Fine and coarse particulate air
1019 pollution in relation to respiratory health in Sweden, *Eur Respir J*, 42(4), 924–934,
1020 <https://doi.org/10.1183/09031936.00088212>, 2013.
- 1021 Wilson, R. and Spengler, J. D., Eds.: *Particles in our air: concentrations and health effects*, Harvard School of Public Health ;
1022 distributed by Harvard University Press, Cambridge, Mass., 1996.
- 1023 Yan, Y., He, Q., Guo, L., Li, H., Zhang, H., Shao, M. and Wang, Y.: Source apportionment and toxicity of atmospheric
1024 polycyclic aromatic hydrocarbons by PMF: Quantifying the influence of coal usage in Taiyuan, China, *Atmospheric Research*,
1025 193, 50–59, <https://doi.org/10.1016/j.atmosres.2017.04.001>, 2017.
- 1026 Yang, F., Kawamura, K., Chen, J., Ho, K., Lee, S., Gao, Y., Cui, L., Wang, T. and Fu, P.: Anthropogenic and biogenic organic
1027 compounds in summertime fine aerosols (PM_{2.5}) in Beijing, China, *Atmospheric Environment*, 124, 166–175,
1028 <https://doi.org/10.1016/j.atmosenv.2015.08.095>, 2016.
- 1029 Yang, X., Feng, L., Zhang, Y., Hu, H., Shi, Y., Liang, S., Zhao, T., Fu, Y., Duan, J. and Sun, Z.: Cytotoxicity induced by fine
1030 particulate matter (PM_{2.5}) via mitochondria-mediated apoptosis pathway in human cardiomyocytes, *Ecotoxicology and
1031 Environmental Safety*, 161, 198–207, <https://doi.org/10.1016/j.ecoenv.2018.05.092>, 2018.
- 1032 Yuan, Z., Lau, A., Zhang, H., Yu, J., Louie, P. and Fung, J.: Identification and spatiotemporal variations of dominant PM₁₀
1033 sources over Hong Kong, *Atmospheric Environment*, 40(10), 1803–1815, <https://doi.org/10.1016/j.atmosenv.2005.11.030>,
1034 2006.
- 1035 Zhang, Y., Müller, L., Winterhalter, R., Moortgat, G. K., Hoffmann, T. and Pöschl, U.: Seasonal cycle and temperature
1036 dependence of pinene oxidation products, dicarboxylic acids and nitrophenols in fine and coarse air particulate matter, *Atmos.
1037 Chem. Phys. Discuss.*, 10(5), 13253–13286, <https://doi.org/10.5194/acpd-10-13253-2010>, 2010.
- 1038 Zhang, Y., Tang, L., Sun, Y., Favez, O., Canonaco, F., Albinet, A., Couvidat, F., Liu, D., Jayne, J. T., Wang, Z., Croteau, P.
1039 L., Canagaratna, M. R., Zhou, H., Prévôt, A. S. H. and Worsnop, D. R.: Limited formation of isoprene epoxydiols-derived
1040 secondary organic aerosol under NO_x-rich environments in Eastern China: LIMITED FORMATION OF IEPOX-SOA,
1041 *Geophys. Res. Lett.*, <https://doi.org/10.1002/2016GL072368>, 2017.
- 1042 Zheng, J., Tan, M., Shibata, Y., Tanaka, A., Li, Y., Zhang, G., Zhang, Y. and Shan, Z.: Characteristics of lead isotope ratios
1043 and elemental concentrations in PM₁₀ fraction of airborne particulate matter in Shanghai after the phase-out of leaded gasoline,
1044 *Atmospheric Environment*, 38(8), 1191–1200, <https://doi.org/10.1016/j.atmosenv.2003.11.004>, 2004.

1045 Zhu, Y., Huang, L., Li, J., Ying, Q., Zhang, H., Liu, X., Liao, H., Li, N., Liu, Z., Mao, Y., Fang, H. and Hu, J.: Sources of
1046 particulate matter in China: Insights from source apportionment studies published in 1987–2017, *Environment International*,
1047 115, 343–357, <https://doi.org/10.1016/j.envint.2018.03.037>, 2018.

1048